Distinct cellular expression and subcellular localization of Kv2 voltage-gated K^+ channel subtypes in dorsal root ganglion neurons conserved between mice and humans

Robert G. Stewart[1], Miriam Camacena[1], Bryan A. Copits[2], Jon T. Sack[1,3]

Affiliations:

[1] Department of Physiology and Membrane Biology, University of California Davis, Davis, CA 95616, USA.

[2] Washington University Pain Center, Washington University School of Medicine, St. Louis, MO 63110, USA; Department of Anesthesiology, Washington University School of Medicine, St. Louis, MO 63110, USA.

[3] Department of Anesthesiology and Pain Medicine, University of California Davis, Davis, CA 95616, USA.

Corresponding author email: jsack@ucdavis.edu

Number of figures: 10

Number of supplemental figures: 15

Number of tables: 2

Conflict of interest statement: The authors declare no competing conflicts of interest.

Data availability: The data that support the findings of this study are available upon request from the authors. Code used to analyze this data in ImageJ and R is available at https://github.com/SackLab/DRG-Image-Processing

Running Title: Kv2 localization in DRG neurons

Keywords: Dorsal root ganglion, Voltage gated ion channels, Kv2.1, Kv2.2, Somatosensory neurons

Acknowledgments:

We thank James S. Trimmer (University of California, Davis) for generous provision of antibodies, numerous discussions, and feedback on the manuscript. We thank Michael Ferns (University of California, Davis) for feedback on the manuscript. We thank the human tissue donors and their families for their generous donations to science. We thank Jiwon Yi, Zack Bertels, Maria Payne, and Jon Lemen for performing hDRG extractions. GxTX was synthesized at the Molecular Foundry of the U.S. Department of Energy under contract DE-AC02-05CH11231. This research was supported by U.S. National Institutes of Health grant R01NS096317 to J.T. Sack and the University of California, Davis.

Author contributions: R. G. Stewart: Conceptualization, formal analysis, investigation, methodology, visualization, writing-original draft, writing-reviewing and editing. M. Camacena: investigation. B. A. Copits investigation, writing-reviewing and editing. J.T. Sack: Conceptualization, formal analysis, funding acquisition, investigation, methodology, project administration, supervision, visualization, writing-original draft, writing-reviewing and editing.

ABSTRACT

The distinct organization of Kv2 voltage-gated potassium channels on and near the cell body of brain neurons enables their regulation of action potentials and specialized membrane contact sites. Somatosensory neurons have a pseudounipolar morphology and transmit action potentials from peripheral nerve endings through axons that bifurcate to the spinal cord and the cell body within ganglia including the dorsal root ganglia (DRG). Kv2 channels regulate action potentials in somatosensory neurons, yet little is known about where Kv2 channels are located. Here we define the cellular and subcellular localization of the Kv2 paralogs, Kv2.1 and Kv2.2, in DRG somatosensory neurons with a panel of antibodies, cell markers, and genetically modified mice. We find that relative to spinal cord neurons, DRG neurons have similar levels of detectable Kv2.1, and higher levels of Kv2.2. In older mice, detectable Kv2.2 remains similar while detectable Kv2.1 decreases. Both Kv2 subtypes adopt clustered subcellular patterns that are distinct from central neurons. Most DRG neurons co-express Kv2.1 and Kv2.2, although neuron subpopulations show preferential expression of Kv2.1 or Kv2.2. We find that Kv2 protein expression and subcellular localization is similar between mouse and human DRG neurons. We conclude that the organization of both Kv2 channels is consistent with physiological roles in the somata and stem axons of DRG neurons. The general prevalence of Kv2.2 in DRG as compared to central neurons and the enrichment of Kv2.2 relative to detectable Kv2.1, in older mice, proprioceptors, and axons suggest more widespread roles for Kv2.2 in DRG neurons.

56 **Significance statement**

57

58 The subcellular distribution of Kv2 voltage-gated potassium channels enable compartment-
59 specific modulation of membrane excitability and organization of membrane contact sites. Here
60 we identify subcellular distributions of the Kv2 paralogs, Kv2.1 and Kv2.2, in somatosensory
61 neurons that bear similarities to and distinctions from central neurons. The distribution of Kv2
62 channels is similar in mouse and human somatosensory neurons. These results identify unique
63 locations of Kv2 channels in somatosensory neurons that could enable roles in sensory
64 information processing.

65 **INTRODUCTION**

66

67 The subcellular localization of voltage-gated ion channels determines how electrical signals are
68 propagated. The two members of the Kv2 family of voltage gated potassium channels, Kv2.1 and Kv2.2,
69 are important for modulating electrical signals in mammalian somatosensory neurons (Bocksteins et al.,
70 2009; Lee et al., 2020; Sun et al., 2022; Tsantoulas et al., 2014; Zheng et al., 2019), yet little is known
71 about where Kv2 channels are localized in these neurons. In central neurons, Kv2 channels are
72 sequestered to specific subcellular regions and identification of where these channels are has helped
73 elucidate their functional roles (Bishop et al., 2015; Du, Tao-Cheng, Zerfas, & McBain, 1998; Irie, 2021;
74 Jensen et al., 2017; Johnson et al., 2018; Kihira, Hermanstyne, & Misonou, 2010; Kirmiz, Vierra, Palacio,
75 & Trimmer, 2018; Misonou, Mohapatra, Menegola, & Trimmer, 2005; Muennich & Fyffe, 2004; Romer et
76 al., 2014; Scannevin, Murakoshi, Rhodes, & Trimmer, 1996; Trimmer, 1991; Vierra, O'Dwyer,
77 Matsumoto, Santana, & Trimmer, 2021). Establishing where Kv2 channels are in somatosensory neurons
78 likewise identifies sites where they could function.

79

80 Among vertebrates, the Kv2 family contains two conserved paralogs, Kv2.1 and Kv2.2, which can
81 assemble into homo- or hetero-tetramers to form voltage gated K^+ channels (Blaine & Ribera, 1998;
82 Kihira et al., 2010). In central neurons, Kv2.1 and Kv2.2 channels have unique cellular expression,
83 subcellular localization, and show distinct physiological roles (Bishop et al., 2015; Newkirk et al., 2022).
84 Among cortical neuron types, Kv2.1 is more broadly distributed than Kv2.2 (Bishop et al., 2015). Little is
85 known of how Kv2.1 or Kv2.2 channels are distributed among somatosensory neuron subtypes. In
86 central neurons, Kv2.1 and Kv2.2 channels localize in clusters on the cell soma, proximal dendrites, and
87 axon initial segment (Bishop et al., 2015; King, Manning, & Trimmer, 2014; Sarmiere, Weigle, & Tamkun,
88 2008; Scannevin et al., 1996; Trimmer, 1991). Clustered Kv2 channels form endoplasmic reticulum-

89 plasma membrane junctions (Johnson et al., 2018; Kirmiz et al., 2018), where they perform
90 nonconducting functions which include mediating coupling of L-type calcium channels to ryanodine
91 receptors (Vierra et al., 2021), and Ca^{2+} uptake (Panzera et al., 2022). In somatosensory neurons it
92 remains unknown whether Kv2 channels form organized structures or are localized to specific
93 subcellular compartments. Identifying if channel expression is specific to neuron subtypes and within
94 specific subcellular domains could indicate whether Kv2.1 and Kv2.2 channels also have distinct
95 physiological roles in somatosensory neurons.
96
97 Kv2 channels are expressed and play important functional roles in DRG. Kv2 transcripts have been
98 detected in all classes of DRG neurons with a notable absence of Kv2.1 mRNA in proprioceptors (Usoskin
99 et al., 2015; Wangzhou et al., 2020; Zheng et al., 2019). Presence of Kv2.1 protein in DRG of mice and
100 rats has been identified by western blot and immunohistochemistry respectively (Sun et al., 2022;
101 Tsantoulas et al., 2012). Pharmacological inhibition of Kv2 channels enhances rat DRG neuron
102 responsiveness to sustained inputs (Tsantoulas et al., 2014). Kv2 conductances have been identified in
103 several mouse DRG neuron subtypes (Bocksteins et al., 2009; Regnier, Bocksteins, Van de Vijver,
104 Snyders, & van Bogaert, 2016; Zheng et al., 2019). Kv2 channels have also been implicated in
105 nociception. Kv2.1 and Kv2.2 mRNA transcript levels are decreased after peripheral axotomy of rat DRG
106 neurons (Tsantoulas et al., 2014). Suppression of Kv2.1 transcription by the epigenetic factor Cdyl is
107 implicated in regulating pain sensation (Sun et al., 2022). A missing piece of the puzzle of how Kv2
108 channels are involved in somatosensory neuron function is the location of the channels themselves.
109 Here we use antibodies against Kv2.1 and Kv2.2 to define their cellular expression and subcellular
110 localization in DRG neurons of both mice and humans.

111 **MATERIALS AND METHODS**

112

113 ***Mice***

114 This study was approved by the UC Davis Institutional Animal Care and Use Committee and conforms to
115 guidelines established by the NIH. Mice were maintained on a 12 h light/dark cycle, and food and water
116 was provided *ad libitum.* Kv2.1 KO and Kv2.2 KO mice were from breeding Kv2.1+/- or Kv2.2+/-
117 heterozygous mice such that WT mice were from breeding pairs that generated KO mice. Kv2.1 and Kv2.2
118 DKO mice were generated from breeding Kv2.1+/- heterozygous and Kv2.2-/- homozygous mice. WT
119 controls for Kv2.1/Kv2.2 DKO experiments were C57BL/6J mice purchased from Jackson Laboratory (stock
120 #000664). The PV^{Ai14} mouse line was a generous gift from Dr. Theanne Griffith (University of California
121 Davis, Davis CA) and were a cross of $Rosa26^{Ai14}$ (stock #007914, MGI: J:155793) and *PVcre* (stock #008069,
122 MGI:J: 100886) mice. The $MrgprD^{GFP}$ mouse line was a generous gift from Dr. David Ginty (Harvard
123 University, Boston MA) (MGI: 3521853). Detailed information about the genotype, age, sex and level of
124 spinal column of mice used in each figure can be found in Table 1.

125

126 ***Human Tissue Collection***

127 Human DRG were obtained in collaboration with Mid-America Transplant (St. Louis, MO) from three
128 donors. Donor #1 was a 59-year-old Caucasian male and the DRG was from the 2nd lumbar region (cause
129 of death: anoxia/stroke). Donor #2 was a 59-year-old black male and the DRG was from the 3rd lumbar
130 region (cause of death: hemorrhagic stroke). Donor #3 was a 58-year-old Caucasian female and the DRG
131 was from the 3rd lumbar region (cause of death: cerebrovascular/stroke). DRG were extracted less than
132 2 hours after aortic cross clamp and transported to the lab where they were dissected to remove the
133 dura, embedded in Optimal Cutting Temperature (OCT) compound, snap frozen, and stored at -80 °C

134 until use (Valtcheva et al., 2016). Human DRG were obtained from organ donors with full legal consent
135 for use of tissue for research in compliance with procedures approved by Mid-America Transplant.
136
137 ***Tissue Preparation***
138 Mice were briefly anesthetized with 3-5% isoflurane and then decapitated. The spinal column was
139 dissected, and excess muscle tissue removed. The spinal column was then bisected in the middle of the
140 L1 vertebrae identified by the 13th rib and drop fixed for 1 hour in ice cold PFA: 4% formaldehyde
141 prepared fresh from paraformaldehyde in 0.1 M phosphate buffer (PB) pH adjusted to 7.4 with NaOH.
142 0.1 M PB buffer was diluted from a 0.4 M PB stock solution that was made by diluting 91.37 g of
143 $Na_2H_2PO_4$ and 20.98 g of $Na_2H_2PO_4 \bullet H_2O$ in 2 liters of milliQ water. The relatively short fixation period
144 was chosen because a longer fixation period increased the off target secondary antibody
145 immunofluorescence from mouse isotype secondary antibodies (Supplemental Figure 1). The spine was
146 washed 3× for 10 min each wash in PB and cryoprotected at 4 °C in 30% sucrose in PB for 24 hours. The
147 spine was cut into sections containing two vertebra per sample which were frozen in OCT (Fisher
148 cat#4585) and stored at -80 °C until sectioning. Vertebrae position relative to the 13th rib was recorded
149 for each frozen sample to determine the specific vertebrae position in the spinal cord. Samples were cut
150 into 30 µm sections on a freezing stage sliding microtome and were collected on Colorfrost Plus
151 microscope slides (Fisher cat#12-550-19). Slides were stored at -20 °C or immediately used for multiplex
152 immunofluorescence labeling.
153
154 Human DRG were cut into 30 µm sections on a freezing stage sliding microtome and were collected on
155 Colorfrost Plus microscope slides. Sections were briefly thawed to adhere to the slide but were
156 immediately returned to the cryostat kept at -20 °C. Slides were removed from the cryostat and
157 immediately transferred to freshly made 4% PFA pH 7.4 for 10 minutes. Slides were then placed in PB

158 solution for 10 minutes and immediately used for multiplex immunofluorescence labeling. Attempts at
159 immunolabeling Kv2 channels in human DRG tissue that was fixed in 4% PFA for 24 hours were not
160 successful.
161
162 ***Neuron Cell Culture***
163 Cervical, thoracic and lumbar DRGs were harvested from mice and transferred to Hank's buffered saline
164 solution (HBSS) (Invitrogen). Ganglia were treated with collagenase (2 mg/ml; Type P, Sigma-Aldrich) in
165 HBSS for 15 min at 37°C followed by 0.05% Trypsin-EDTA (Gibco) for 2.5 min with gentle rotation. Trypsin
166 was neutralized with culture media (MEM, with L-glutamine, Phenol Red, without sodium pyruvate)
167 supplemented with 10% horse serum (heat-inactivated; Gibco), 10 U/ml penicillin, 10 µg/ml streptomycin,
168 MEM vitamin solution (Gibco), and B-27 supplement (Gibco). Serum-containing media was decanted and
169 neurons were triturated using a fire-polished Pasteur pipette in MEM culture media containing the
170 supplements listed above. Neurons were plated on laminin-treated (0.05 mg/ml, Sigma-Aldrich) 35 mm
171 glass bottom dishes (MatTek cat#P35G-1.5-7-C). Neurons were then incubated at 37°C in 5% CO_2. Neurons
172 were used for imaging experiments within 24 hours after plating.
173
174 ***Labeling Endogenous Kv2 in live cultured DRG neurons***
175 Plates were removed from 37°C incubator 24 hours after plating. Neurons were washed once with 1 mL
176 neuronal external (NE) solution (3.5 KCl, 155 NaCl, 10 HEPES, 1.5 CaCl2, and 1 MgCl2, 10 mM glucose
177 adjusted to pH 7.4 with NaOH). Neurons were then incubated with NE solution supplemented with 1%
178 BSA for 5 minutes. Neurons were then washed once with NE solution and incubated in 5 µg/mL wheat
179 germ agglutinin conjugated to Alexa Fluor 405 (Biotium cat#29028-1) diluted in NE solution for 2.5
180 minutes. Neurons were washed twice with NE solution and imaged. NE solution was removed and then
181 neurons were incubated for 10 minutes in 100 nM GxTX-594 prepared as described (Thapa et al., 2021).

182 Neurons were then washed three times in NE solution and imaged again. The temperature of the
183 imaging chamber was 25 °C throughout the experiment. Experimenter was blinded to which culture
184 dishes contained DRG neurons from either WT or Kv2.1/Kv2.2 double knockout mice throughout the
185 experiment and image analysis.
186
187 ***Immunohistochemistry***
188 A hydrophobic barrier was drawn around tissue sections mounted on slides as described above using a
189 hydrophobic barrier pen (Scientific Device cat#9804-02). Sections were incubated in 4% milk, 0.1 M
190 phosphate buffer (PB) and 0.2% Triton X-100 (vehicle) for 1 hour. Sections were then incubated in
191 vehicle containing 0.1 mg/mL IgG F(ab) polyclonal IgG antibody (Abcam cat#ab6668) for 1 hour. We
192 determined that a concentration of 0.1 mg/mL maximally blocked off-target secondary antibody labeling
193 when using isotype-specific anti-mouse secondary antibodies (Supplemental Figure 2). Sections were
194 washed 3× for 5 min each in vehicle and then incubated in vehicle containing primary antibodies for 1
195 hour. Primary antibodies and concentrations used are listed in Table 2. Sections were then washed 3×
196 for 5 min each in vehicle and then incubated in vehicle containing IgG-subclass-specific secondary Abs
197 for one hour (Thermo Fisher). Sections were then washed 3× for 5 min each in PB and mounted with
198 Prolong Gold (Thermo Fisher cat#P36930) and Deckglaser cover glass (Fisher Scientific cat#NC1776158).
199 All incubations and washes were done at room temperature with gentle rocking. Human tissue was
200 immunolabeled identically to mice with the exception that the step incubating sections in vehicle
201 containing 0.1 mg/mL IgG F(ab) polyclonal IgG antibody was omitted and sections were incubated in
202 primary antibodies for 2 hours instead of 1. Primary antibodies used in Figure 2 and Figure 3 were used
203 at saturating concentrations (Supplemental Figure 4).
204
205 ***Imaging***

206 Images were acquired with an inverted scanning confocal and airy disk imaging system (Zeiss LSM 880
207 Airyscan, 410900-247-075) run by ZEN black v2.1. Laser lines were 405 nm, 488 nm, 543 nm and 633 nm.
208 Low-magnification images to image whole mouse DRG were acquired in confocal or airy disk imaging
209 mode with a 0.8 NA 20x objective (Zeiss 420650-9901) details in figure legends. Images containing both
210 the DRG and spinal cord were tile scan images acquired in confocal mode with the same 20x objective.
211 When imaging whole DRG for Figure 2 and Figure 3 the imaging plane was selected using fluorescence
212 from channels that did not contain anti-Kv2.1 or anti-Kv2.2 immunofluorescence. High-magnification
213 images were acquired in airy disk imaging mode with a 1.4 NA 63x oil objective (Zeiss 420782-9900-799).
214 Linear adjustments to contrast and brightness and average fluorescence intensity z-projections were
215 performed using ImageJ software.

216

217 ***Image Analysis***

218 Images were analyzed using ImageJ software (Schindelin et al., 2012). A summary of automated analysis
219 for selecting neurons in DRG sections can be found in Supplemental Figure 5. The ImageJ plugin
220 MorphoLibJ was used for performing watershed segmentation of images (Legland, Arganda-Carreras, &
221 Andrey, 2016). Automatic generation of ROIs from watershed segmentation did not distinguish the
222 presence of nuclei and is thus expected to over-count larger diameter neurons. Unless stated otherwise
223 the region of DRG neurons used to analyze anti-Kv2 immunofluorescence is the outer edge
224 (Supplemental Figure 5 I). Immunofluorescence is defined as the raw pixel values from confocal images
225 and was not background subtracted. We noted that in smaller neurons the nucleus takes up a greater
226 percentage of the total volume and could skew fluorescence measurements if fluorescence in the entire
227 soma volume is measured. As Kv2 protein is not present in the nucleus and is enriched at the outer edge
228 (Figure 1) we found that measuring anti-Kv2 immunofluorescence at the outer edge of the neuron
229 reduces potential error that could be associated with soma diameter. For proteins that were not Kv2

230 channels we analyzed the immunofluorescence of the entire soma as these proteins did not exhibit the

231 same enrichment at the outer edge as Kv2 channels (Figure 9 B). Where specified, manual ROIs were

232 used in analysis otherwise automatically generated ROIs were used. When analyzing

233 immunofluorescence from human neurons, ROIs were drawn around areas within the neuronal soma

234 that do not contain apparent lipofuscin (Supplemental Figure 11 C). Fitting of imaging data was

235 performed using Igor Pro software version 8 (Wavemetrics, Lake Oswego, OR) that employs nonlinear

236 least square curve fitting via the Levenberg-Marquardt algorithm. Distributions of fluorescence intensity

237 from DRG neurons were fit with a log normal distribution:

238

239 $$f(x) = A^{-\left[\frac{\ln\left(\frac{x}{x_0}\right)}{width}\right]^2} \qquad \text{(Equation 1)}$$

240

241 Where A = amplitude, x_0 = mean, and width = $\sqrt{2}$ times standard deviation. Concentration-effect

242 experiments in Supplemental Figure 4 were fit with the Hill equation:

243

244 $$f(x) = base + \frac{max - base}{1 + \left(\frac{x_{half}}{x}\right)^n} \qquad \text{(Equation 2)}$$

245

246 ***Code Accessibility***

247 In-house Fiji macros and R script used to process imaging data are available for download at

248 https://github.com/SackLab/DRG-Image-Processing

249

250 ***Statistics***

251 All statistical tests were performed in Igor Pro software version 8 (Wavemetrics, Lake Oswego, OR).

252 Independent replicates (n) are individual neurons while biological replicates (N) are individual mice. The

253 n and N values for each figure are listed in Table 1. Details of statistical tests are in the figure legends.

254 We did not observe a difference between males and females in detectable Kv2.1 or Kv2.2 protein, but

255 animal numbers were not sufficient for rigorous statistical comparison.

256 **RESULTS**

257

258 **Kv2.1 and Kv2.2 immunolabeling is enriched at the apparent plasma membrane of DRG neuron**

259 **somata**

260

261 To assess the cellular expression and subcellular localization of Kv2.1 and Kv2.2 voltage gated potassium

262 channels in DRG neurons we used a set of anti-Kv2.1 and anti-Kv2.2 antibodies that have previously

263 been validated in brain tissue from Kv2 knockout mice (Bishop et al., 2015) to perform multiplex

264 immunofluorescence labeling of DRG neurons. Anti-Kv2.1 (magenta) and anti-Kv2.2 (green)

265 immunofluorescence is prominent in DRG neuron somata (Figure 1 A). In neurons we observed anti-

266 Kv2.1 and anti-Kv2.2 immunofluorescence enriched at the outer edge of DRG neuron somata consistent

267 with their plasma membrane localization (Figure 1 B arrows). This putative cell surface localization is

268 distinct from prior reports of anti-Kv2 immunofluorescence in DRG (Tsantoulas et al., 2012) as well as

269 that for other ion channel proteins such as Nav1.8 (Shields et al., 2012) and TRPV1 (Cho & Valtschanoff,

270 2008), all of which are primarily in the cytoplasm. Anti-Kv2.1 or anti-Kv2.2 immunofluorescence at the

271 edge of neuron somata was more apparent when imaging thinner optical sections. To determine if

272 enrichment of Kv2 immunolabeling at the outer edge of DRG neurons was an artifact of our

273 immunohistochemistry or imaging protocols, we additionally labeled DRG sections with a knockout-

274 validated antibody against Nav1.8. In the same DRG section labeled for Kv2 channels, cytoplasmic anti-

275 Nav1.8 immunofluorescence was prominent in small to medium diameter lumbar DRG neurons,

276 consistent with previous reports (He et al., 2010; Shields et al., 2012) (Figure 1 B). To quantify

277 enrichment of anti-Kv2 versus anti-Nav1.8 immunofluorescence at the outer edge of DRG neurons, we

278 manually drew regions of interest (ROIs) for each DRG soma. We generated a 2 µm wide annulus that

279 encompassed the outer edge and a second 2 µm wide annulus just inside the first one (Figure 1 C arrows

280 1 and 2 respectively). By comparing the fluorescence intensity of immunofluorescence signals within
281 these annuli we found that the edge of DRG neuron somata is enriched for anti-Kv2.1 and anti-Kv2.2
282 immunofluorescence relative to that of Nav1.8 (ANOVA < 0.001) (Figure 1 D). Similarly, anti-Kv2.1 and
283 anti-Kv2.2 immunofluorescence is enriched at the edge of DRG neuron somata relative to anti-TRPV1
284 immunofluorescence (ANOVA < 0.001) (Supplemental Figure 3).
285
286 **The majority of dorsal root ganglion neurons express Kv2 protein**
287
288 To determine whether the anti-Kv2.1 immunofluorescence signal in DRG sections is specific and
289 dependent on the presence of Kv2.1 protein, we compared fluorescence intensities in DRG samples
290 prepared in parallel from age and sex matched wild-type (WT) mice and Kv2.1 knock-out (KO) mice. We
291 observed anti-Kv2.1 immunolabeling in WT DRG neurons that was absent from Kv2.1 KO, while
292 fluorescence corresponding to an antibody that targets βIII tubulin was similar in both WT and Kv2.1 KO
293 mice (Figure 2 A). To quantify fluorescence intensities of DRG sections, we manually drew ROIs around
294 neuron soma profiles with clearly visible nuclei and measured the fluorescence intensity at the outer
295 edge of profiles as shown in Figure 1 C. We define a profile as a slice of a DRG neuron in a histological
296 section (Coggeshall, 1992). We found that 99% of manually identified profiles from the WT mouse DRG
297 shown in Figure 2 A had anti-Kv2.1 immunofluorescence above the mean of Kv2.1 KO mice (Figure 2 B).
298 To reduce human bias in identification of profiles we used an automated method to generate ROIs. As
299 with the manual method, the automated method reliably identified neuronal profiles (Supplemental
300 Figure 5 I). However, the automated method did not distinguish profiles without nuclei which could lead
301 to overrepresentation of larger neurons (Coggeshall, 1992; Coggeshall & Lekan, 1996). Additionally, the
302 automated method occasionally selected ROIs which did not appear to be neurons (Supplemental Figure
303 5 H red arrows). Despite these limitations, the absolute reproducibility of the automated method when

304 scaled to identify thousands of neuronal profiles indicated that automated ROIs could provide a rigorous
305 means of identifying neuronal profiles for statistical analysis. In automatically generated ROIs from the
306 same WT mouse manually analyzed in Figure 2 B we observed a reduction in the mean anti-Kv2.1 but
307 not anti-βIII immunofluorescence in Kv2.1 KO mice (Figure 2 C and D). We found that 89% of
308 automatically generated ROIs had anti-Kv2.1 immunofluorescence above the mean of the paired Kv2.1
309 KO mouse. We manually identified that 9% of the automatically generated ROIs from the WT mouse did
310 not appear to be neurons, suggesting that 98% of profiles in this automated dataset could have anti-
311 Kv2.1 immunofluorescence above the mean of the Kv2.1 KO mouse, consistent with manual analysis.
312 We expanded the automated method to 5 pairs of age and sex matched WT and Kv2.1 KO mice, and
313 found that anti-Kv2.1 immunofluorescence was significantly reduced in each matched Kv2.1 KO mouse
314 relative to anti-Kv2.2 or anti-βIII tubulin immunofluorescence while no significant difference was
315 observed between anti-Kv2.2 and anti-βIII tubulin (Figure 2 E) (ANOVA $p < 0.001$). We identified that 93
316 ± 6% (SD) of ROIs from the five WT mice had anti-Kv2.1 immunofluorescence above the mean of age and
317 sex matched Kv2.1 KO mice (Figure 2 F). This analysis confirms that anti-Kv2.1 immunofluorescence
318 reveals Kv2.1 protein at neuron surfaces.
319
320 We developed a method to estimate the fraction of ROIs that contain detectable Kv2.1 protein. The
321 histogram of fluorescence intensity in automatically generated ROIs from Kv2.1 KO DRG sections labeled
322 with an anti-Kv2.1 antibody had variability which could reasonably be fit with a log normal distribution
323 (equation 1) (Figure 2 G). We assumed a similar distribution of background immunofluorescence is also
324 present in neuron profiles of age and sex matched WT mice and fit the Kv2.1 KO distribution to the WT
325 histogram to estimate the fraction of ROIs without detectable Kv2.1 (Figure 2 H red gaussian). Using this
326 method, we compared Kv2.1 immunofluorescence in DRG sections of multiple age and sex matched WT
327 and Kv2.1 KO mice. The fitting indicated that 84 ± 9% (SD) of automatically generated ROIs from WT

328 mice have detectable Kv2.1 protein (N = 5 pairs of mice) (Figure 2 I). As approximately 9% of ROIs are
329 expected to not contain neurons these results suggest that greater than 90% of mouse DRG neurons
330 have detectable Kv2.1 protein. We further validated our automated methodology with a transgenic
331 MrgprD-GFP mouse line that expresses GFP in non-peptidergic nociceptors that comprise approximately
332 19-24% of all lumbar DRG neurons (Dirajlal, Pauers, & Stucky, 2003; Dong, Han, Zylka, Simon, &
333 Anderson, 2001; Wang & Zylka, 2009). In comparing the MrgprD-GFP mice to WT C57BL/6J mice we
334 found that 23 ± 15% (SD) of automatically generated profiles (N = 4 pairs of mice) had detectable GFP
335 (Supplemental Figure 6).
336
337 We compared anti-Kv2.2 immunofluorescence from an age and sex matched WT and Kv2.2 KO mouse by
338 drawing ROIs around neuron soma profiles with clearly visible nuclei. This identified that greater than
339 99% of WT profiles have anti-Kv2.2 immunofluorescence above the mean immunofluorescence of the
340 paired Kv2.2 KO mouse (Figure 3 B). Automatically generated ROIs for multiple age and sex matched WT
341 and Kv2.2 KO mice indicate that 91 ± 5% (SD) of ROIs from WT mice have detectable Kv2.2 protein (N = 8
342 pairs of mice) (Figure 3 F-H). Using the automated analysis, we found that anti-Kv2.2
343 immunofluorescence was significantly reduced in Kv2.2 KO mice relative to anti-Kv2.1 or anti-NF200
344 immunofluorescence in age and sex matched WT and Kv2.2 KO mice (ANOVA $p < 0.001$) while no
345 significant difference between anti-NF200 or anti-Kv2.1 immunofluorescence was observed (Figure 3 A-
346 E). These combined results suggest that more than 90% of neuron profiles contain detectable Kv2.1 or
347 Kv2.2 protein, raising the possibility that all mouse DRG neurons express Kv2 channels.
348

349 **Kv2.1 immunolabeling decreases in older mice while Kv2.2 immunolabeling remains similar**

350

351 Kv2.2 transcript in mouse DRG decreases during postnatal development (Regnier et al., 2016) and Kv2.1
352 protein expression in mouse brain decreases with age (Cotella et al., 2012; Regnier et al., 2016). To
353 identify if Kv2 protein levels in DRG neurons vary between young adult and old mice we compared anti-
354 Kv2.1 and anti-Kv2.2 immunofluorescence from samples subjected to identical immunolabeling and
355 imaging protocols. We observed lower anti-Kv2.1 (Figure 4 A, B and C) in DRG sections from 50 week old
356 mice relative to 7-16 week old mice. Comparisons with Kv2.1 KO mice indicate that 50 ± 23% (SD) of
357 ROIs from 50 week old mice express detectable Kv2.1 protein, significantly less (p = 0.018) than the 84 ±
358 9% (SD) of ROIs with detectable Kv2.1 protein from 7-16 week old mice (Figure 4 D). In contrast, similar
359 anti-Kv2.2 immunofluorescence was seen in samples from young adult and old mice (Figure 4 E, F and
360 G). Comparisons with Kv2.2 KO mice indicate that 96 ± 3% of profiles from 50 week old mice express
361 detectable Kv2.2 protein, a weakly significant increase (p = 0.03) from the 88 ± 3% (SD) of profiles with
362 detectable Kv2.2 protein from 7-24 week old mice (Figure 4 H). We note that this weak statistical
363 increase is underpowered due to the availability of only three 50 week old Kv2.2 KO mice.

364

365 **Kv2 channels are expressed on the cell surface of acutely dissociated DRG neurons**

366

367 To determine if Kv2 channels are present on neuron surfaces we labeled live acutely dissociated DRG
368 neurons with a cell-impermeant fluorescent probe which binds Kv2 channels. The probe is a variant of
369 the tarantula peptide guangxitoxin-1E conjugated to Alex Fluor 594 (GxTX-594) which binds to an
370 extracellular site of Kv2.1 and Kv2.2 channels (Thapa et al., 2021). We applied GxTX-594 to live
371 dissociated DRG neurons from WT mice and double knockout (DKO) mice lacking expression of both
372 Kv2.1 and Kv2.2 protein (Figure 5). In WT DRG neurons, we observed fluorescence at the membrane

373 after application of 100 nM GxTX-594 that was not present before the addition of GxTX-594 (Figure 5 A).
374 Wheat germ agglutinin conjugated to Alexa 405 (WGA-405) was used to identify the surface membrane
375 of cultured DRG neurons and confirmed that the GxTX-594 fluorescence observed in WT neurons was
376 cell surface localized (Figure 5 A middle). The cell surface localized fluorescence of GxTX-594 observed in
377 WT neurons was not present in Kv2.1/Kv2.2 DKO neurons (Figure 5 B). To quantify the cell surface-
378 associated fluorescence signals of individual WT and Kv2.1/Kv2.2 DKO neurons, we used an automated
379 method to generate ROIs corresponding to the WGA-405 fluorescence and measured GxTX-594 labeling
380 within this ROI (Figure 5 C). This analysis confirmed a reduction in GxTX-594 fluorescence at the
381 membrane in cultured DRG neurons from Kv2.1/Kv2.2 DKO mice compared to WT mice (Figure 5 D).
382 Similar to the Kv2 immunofluorescence signals from KO mice (Figures 2 and 3), GxTX-594 fluorescence
383 from Kv2.1 /Kv2.2 DKO mice could be reasonably fit with a log normal distribution (equation 1) (Figure 5
384 E). Applying the same method used to estimate the fraction of neuronal profiles expressing detectable
385 Kv2.1 and Kv2.2 immunofluorescence we compared cultured DRG neurons of age and sex matched WT
386 and Kv2.1/Kv2.2 DKO mice and estimated that 76 ± 2.4% (SD) of DRG neurons have detectable cell
387 surface GxTX-594 fluorescence (Figure 5 F and G). This indicates that at least 76% of neurons express
388 Kv2 channels in their surface membrane, consistent with a report of Kv2 conductance in every DRG
389 neuron type assessed (Zheng et al., 2019) .
390
391 **Anti-Kv2.2 immunofluorescence is enriched in DRG neurons relative to spinal cord neurons**
392
393 In mammals, anti-Kv2.1 and anti-Kv2.2 immunofluorescence is apparent in central neurons of the brain
394 (Kihira et al., 2010; Bishop et al., 2015) and anti-Kv2.1 in the spinal cord (Bishop et al., 2015; Muennich &
395 Fyffe, 2004). We measured Kv2 immunofluorescence intensities in sections of mouse spinal column
396 which contain both the DRG and the spinal cord. Neurons in the ventral and dorsal horn of the spinal

397 cord exhibit anti-Kv2.1 immunofluorescence (Figure 6 A). We observed anti-Kv2.1 puncta on neurons in
398 the ventral horn (Figure 6 A inset) similar to that described in alpha motor neurons (Fletcher et al., 2017;
399 Romer et al., 2014). Fewer spinal cord neurons exhibit anti-Kv2.2 immunofluorescence than anti-Kv2.1
400 (Figure 6 A and Supplemental Figure 7 A arrow heads). Kv2.2 channel protein in the spinal cord of mice
401 has to our knowledge not been assessed, but anti-Kv2.2 immunofluorescence has been observed early
402 in development in the ventrolateral spinal cord in the frog *Xenopus laevis* (Gravagna, Knoeckel, Taylor,
403 Hultgren, & Ribera, 2008). We analyzed anti-Kv2 immunofluorescence from individual neurons in the
404 DRG and ventral horn of five mice and found that while anti-Kv2.1 immunofluorescence is similar
405 between the two regions (Figure 6 B), anti-Kv2.2 immunofluorescence is significantly higher in DRG
406 neurons relative to ventral horn neurons (Figure 6 C). Approximately 30% of neurons in the DRG have
407 anti-Kv2.2 immunofluorescence at a level higher than the brightest anti-Kv2.2 immunofluorescence
408 observed in the spinal cord. We repeated this analysis with a different anti-Kv2.2 antibody and found
409 similar results (Supplemental Figure 7).
410
411 **Kv2 channels on DRG neuron somata and stem axons form clustered subcellular patterns with**
412 **similarities to and distinctions from central neurons.**
413
414 In neurons throughout the brain (Trimmer, 1991, Scannevin et al., 1996, Bishop et al., 2015) and motor
415 neurons in the spinal cord (Muennich and Fyffe, 2004), Kv2 channels form punctate structures referred
416 to as clusters. In central neurons, Kv2 clusters localize to the soma, proximal dendrites and axon initial
417 segment (Lim, Antonucci, Scannevin, & Trimmer, 2000; Scannevin et al., 1996; Trimmer, 1991). At
418 clusters, Kv2 channels organize protein signaling complexes and endoplasmic reticulum-plasma
419 membrane junctions (Johnson et al., 2018; Kirmiz et al., 2018; Panzera et al., 2022; Vierra et al., 2021).
420 To determine whether Kv2 channels in DRG neurons form clusters similar to central neurons, we

421 compared *en face* z-projections of Kv2 clusters in DRG neurons and ventral horn neurons in the same
422 spinal cord section (Figure 7). Anti-Kv2.1 immunofluorescence in the ventral horn neurons of these mice
423 resembles previous reports of mice (Fletcher et al., 2017) and rats (Fletcher et al., 2017; Muennich &
424 Fyffe, 2004). In both DRG and spinal cord neurons, Kv2.1 and Kv2.2 channels form dense clusters (Figure
425 7 A and B). Kv2 channel clusters in DRG typically appeared smaller than Kv2 clusters in spinal cord.
426 However, we are not certain these observations in fixed tissue represent the in vivo arrangement, as
427 Kv2.1 channels in brain neurons can decluster in the period between sacrifice and fixation (Misonou et
428 al., 2005). In some DRG neurons, we observed donut shaped Kv2.1 and Kv2.2 clusters (Figure 7 B and C
429 insets) which resemble donut shaped Kv2 clusters in interneurons which harbor specialized protein
430 machinery in their center (Vullhorst et al., 2015).
431
432 DRG neurons are distinct from central neurons as they have a single stem axon that exits the cell soma
433 and bifurcates into the central and peripheral axon branches (Ha, 1970). We observed punctate
434 immunofluorescence for both Kv2.1 and Kv2.2 on the apparent stem axons of DRG neurons (Figure 7 B,
435 D and E arrow heads, Supplemental Figure 8). In DRG sections from the *MrgprD*^{GFP} mouse line we
436 observed Kv2 clusters on the stem axon of GFP-expressing neurons. As *MrgprD*^{GFP} marks non-peptidergic
437 nociceptors (Zheng et al., 2019) we confirm stem axon localization in this subpopulation of
438 unmyelinated neurons (Supplemental Figure 8 A).
439
440 While Kv2 clusters in central neurons and many DRG neurons are distributed evenly throughout the
441 soma, we found that DRG neurons asymmetrically distribute Kv2 clusters on the soma (Figure 7 B-E
442 arrows). To test if enrichment of Kv2 channel clusters is oriented to a specific region on the soma we
443 manually traced the surface of neurons whose apparent stem axons were visible (Figure 7 F). The
444 brightest anti-Kv2.1 and anti-Kv2.2 immunofluorescence is near the stem axon in 76 and 80% of DRG

445 neurons respectively (Figure 7 G and H). Asymmetric distribution of Kv2 channels is not frequently
446 observed in central neurons of mice (Bishop et al., 2018; Bishop et al., 2015; Romer et al., 2014)
447 suggesting a potentially unique role of Kv2 subcellular organization in DRG neurons.
448
449 **Kv2.2 channels are expressed in peripheral axons of DRG neurons**
450
451 To determine if anti-Kv2 immunofluorescence is detectible in DRG axons in regions beyond the stem
452 axon we immunolabeled samples containing both peripheral and central axons, using NF200 or βIII
453 tubulin as markers for DRG axons which target myelinated neurons or all DRG neurons respectively.
454 Neurons were not co-labeled with βIII tubulin and Kv2.2 targeting antibodies because they were of the
455 same isotype. We did not observe anti-Kv2.1 immunofluorescence in peripheral axons (Supplemental
456 Figure 9) from the same DRG section that had detectable anti-Kv2.1 immunofluorescence in neuron
457 somas (Figure 2). However, anti-Kv2.2 immunofluorescence is detectable in peripheral and central axons
458 of WT but not Kv2.2 KO mice (Figure 8 B and C). Anti-Kv2.2 immunofluorescence on myelinated
459 peripheral axons appears as discrete puncta or as larger bands which span the width of the axon (Figure
460 8 B arrows). We also observed anti-Kv2.2 immunofluorescence not colocalized with NF200, suggestive of
461 unmyelinated fibers (Figure 8 B arrow head). In *MrgprD*^{GFP} mice, anti-Kv2.2 immunofluorescence
462 colocalizes with axons expressing cytosolic GFP, identifying that non-peptidergic nociceptors also
463 express Kv2.2 protein along the peripheral axon (Figure 8 D). We further investigated the expression of
464 Kv2.2 in peripheral myelinated fibers by co-labeling peripheral axons with antibodies specific for CASPR
465 (Einheber et al., 1997) and Kv1.2 (Rasband et al., 1998) which identify the paranodal and juxtaparanodal
466 regions of nodes of Ranvier, respectively in myelinated fibers. We found punctate anti-Kv2.2
467 immunofluorescence associated with both CASPR and Kv1.2 in some WT DRG neuron axons that is not
468 present in Kv2.2 KO mice (Supplemental Figure 10 A). We analyzed anti-Kv2.2 immunofluorescence in

469 WT and Kv2.2 KO mice by manually drawing ROIs around CASPR and Kv1.2 immunofluorescence while
470 blinded to anti-Kv2.2 immunofluorescence and found that 26/34 CASPR and 20/31 Kv1.2
471 immunolabeled regions had anti-Kv2.2 immunofluorescence brighter than the brightest anti-Kv2.2
472 immunofluorescence measured in Kv2.2 KO mice (Supplemental Figure 10 B). These results indicate that
473 Kv2.2 but not Kv2.1 protein is detectable in axons of myelinated and unmyelinated somatosensory
474 neurons. However, these results do not identify if Kv2.2 channels are localized to specific subcellular
475 regions of somatosensory axons.
476
477 **Anti-Kv2.1 and anti-Kv2.2 immunofluorescence is non-uniform across DRG neuron subtypes**
478
479 Different voltage gated potassium channels make distinct contributions to outward potassium currents
480 in sensory neuron subtypes (Zheng et al., 2019). We observed subpopulations of DRG neurons that have
481 bright anti-Kv2.1 immunofluorescence but dim anti-Kv2.2 immunofluorescence and vice-versa (Figure 9
482 A and C, Figure 1 A, and Figure 6 A). We hypothesized that differences in Kv2.1 and Kv2.2 protein density
483 could potentially denote specific subtypes of sensory neurons. In order to test if relative density of Kv2.1
484 and Kv2.2 protein differs in subtypes of DRG neurons, we assessed anti-Kv2.1 and anti-Kv2.2
485 immunofluorescence in four DRG neuron subtypes. Neurons identified by genetically encoded markers
486 were GFP-expressing neurons from *MrgprD*^{GFP} mice which we refer to as non-peptidergic nociceptors
487 (Zheng et al., 2019), or tdTomato-expressing neurons from *PV*^{Ai14} mice which we refer to as
488 proprioceptors (Zheng et al., 2019). Neurons immunolabeled for CGRP we refer to as peptidergic
489 nociceptors (Zheng et al., 2019) and neurons immunolabeled for NF200 we refer to as myelinated DRG
490 neurons (Usoskin et al., 2015) (Figure 9 B and D). We quantified detectable Kv2.1 or Kv2.2 protein
491 density in individual ROIs by rank ordering the immunofluorescence intensity. Rank orders from multiple
492 mice were pooled with a value of 100% representing the brightest ROI in each mouse (Figure 9 D). The

493 rank percentiles of Kv2.1 and Kv2.2 have similar distributions in peptidergic and non-peptidergic
494 nociceptors. Many ROIs with the highest Kv2.1 or Kv2.2 rank percentile were NF200-positive myelinated
495 neurons. Proprioceptors, a subset of the myelinated neurons, appear to account for the subpopulation
496 of neurons with bright anti-Kv2.2 and dim anti-Kv2.1, and have high rank percentiles of Kv2.2 but low
497 rank percentiles of Kv2.1. (Figure 9 A, B, and C). Profiles with bright anti-Kv2.1 and dim anti-Kv2.2
498 immunofluorescence are mostly NF200-positive myelinated neurons of unknown subtype (Figure 9 A, B,
499 and C blue points). Overall, these results identify that the relative densities of Kv2.1 and Kv2.2 protein
500 are similar in DRG neuron subtypes except proprioceptors. These results are consistent with reports that
501 Kv2.1 and Kv2.2 mRNA transcript levels are similar in DRG neuron subtypes except proprioceptors. Our
502 finding that Kv2.1 protein density is anomalously low in proprioceptors mirrors the finding that Kv2.1
503 transcripts are also low in proprioceptors (Usoskin et al., 2015; Zheng et al., 2019).
504
505 **Kv2 channel cellular expression and subcellular localization in human DRG neurons is similar to mice**
506
507 Kv2 mRNA transcripts are present in human DRG neurons (Tavares-Ferreira et al., 2022; Wangzhou et
508 al., 2020), and we assessed whether anti-Kv2 immunofluorescence is associated with human DRG
509 neurons. As human Kv2.1 and Kv2.2 knockout controls are not available, we compared fluorescence in
510 DRG sections with anti-Kv2 primary antibodies to those lacking primary antibodies. Control samples
511 lacking primary antibodies revealed strong autofluorescence at all excitation wavelengths (Supplemental
512 Figure 11 A and B) consistent with other studies of human DRG neurons which have attributed this
513 autofluorescence to lipofuscin (Shiers et al., 2021). We found that most neurons have anti-Kv2.1 and
514 anti-Kv2.2 immunofluorescence brighter than controls lacking primary antibodies (Supplemental Figure
515 11 D and E) suggesting that Kv2 protein is present in human DRG neurons. As a control, we used the
516 same methods with anti-Nav1.7 and anti-Nav1.8 antibodies and found anti-Nav1.7 immunofluorescence

517 in nearly all human DRG neurons while anti-Nav1.8 was in a smaller fraction of DRG neurons, consistent
518 with previous reports of Nav1.7 protein and Nav1.8 transcript in human DRG (Shiers, Klein, & Price,
519 2020) (Supplemental Figure 11 A arrow heads, B, F and G). Similar to DRG neurons in mice, we observed
520 subpopulations of neurons that had bright anti-Kv2.1 immunofluorescence but dim anti-Kv2.2
521 immunofluorescence and conversely neurons that had bright anti-Kv2.2 immunofluorescence but dim
522 anti-Kv2.1 immunofluorescence (Figure 10 A and B). These observations were consistent in DRG from 3
523 human donors (Supplemental Figure 11 A and H and Supplemental Figure 12). We were unable to
524 identify if the population of human DRG neurons with low anti-Kv2.1 and high anti-Kv2.2 are
525 proprioceptors as we observed in mice; attempts to label parvalbumin in human neurons were
526 unsuccessful.
527
528 We assessed whether Kv2 protein subcellular localization in humans is similar to mice. We identified
529 neurons in all three human DRG samples where anti-Kv2.1 and anti-Kv2.2 immunofluorescence was
530 enriched at the outer edge of DRG neuron somata (Figure 10 A arrow and Supplemental Figure 13). In
531 some neurons from all three humans, Kv2 clusters exhibited asymmetric distribution on the neuronal
532 soma (Figure 10 B green arrow head, Supplemental Figure 13 A-E arrows). In one human we identified a
533 neuron with Kv2.2 immunofluorescence that was asymmetrically distributed near the stem axon
534 consistent with observations in mice (Figure 10 B green arrow). We identified Kv2.2
535 immunofluorescence on the stem axon of DRG neurons in all three humans using anti-NF200 or anti-
536 Nav1.7 as markers of the stem axon (Figure 10 B-C and Supplemental Figure 14 arrows). In two out of
537 three humans we also identified Kv2.1 immunofluorescence on the stem axon of human DRG neurons
538 (Figure 10 C inset and Supplemental Figure 14 B and D inset). To determine if Kv2.2 channels are present
539 in human DRG neuron axons, we labeled human DRG sections with the same anti-Kv2.2, anti-NF200,
540 anti-CASPR and anti-Kv1.2 antibodies that were used in mice. We found anti-Kv2.2 immunofluorescence

541 associated with anti-NF200, anti-CASPR and anti-Kv1.2 immunofluorescence in human DRG neuron
542 axons (Supplemental Figure 15) suggesting that Kv2.2 channels could contribute to electrical
543 propagation or other physiological functions in axons of human DRG neurons.
544
545 **DISSCUSSION**
546
547 Our results reveal overlapping yet distinct localization patterns of Kv2.1 and Kv2.2 in DRG neurons. Here,
548 we discuss the unique features of Kv2 localization in the DRG and how these could influence neuronal
549 physiology and somatosensation.
550
551 We identify differences between anti-Kv2.1 and anti-Kv2.2 immunofluorescence in DRG neurons. Kv2.2
552 mRNA is abundant in all DRG neuron subtypes identified, while Kv2.1 mRNA is low in proprioceptors and
553 abundant in other subtypes (Usoskin et al., 2015; Zheng et al., 2019). Consistent with these findings we
554 conservatively estimate that Kv2.1 and Kv2.2 protein is in at least 90% of mouse DRG neurons, though
555 Kv2.1 immunofluorescence is anomalously low in proprioceptors. Detection of Kv2.2 but not Kv2.1 in
556 DRG neuron peripheral and central axons suggests that Kv2.2 channels may be important for electrical
557 transmission in these axons. While detectable Kv2.2 remained constant in DRG neurons of older mice,
558 detectable Kv2.1 decreased, possibly contributing to the altered repolarization noted in DRG neurons
559 from aged mice (Scott, Leu, & Cinader, 1988). The differences between Kv2.1 and Kv2.2 in
560 somatosensory neurons are consistent with distinct roles for these Kv2 paralogs in somatosensory
561 neuron physiology, as seen in brain and pancreatic islets (Bishop et al., 2015; Johnston et al., 2008; Li et
562 al., 2013).
563

564 The expression and subcellular localization of Kv2 channels in DRG neurons are distinct from central
565 neurons. Kv2.1 is present in most brain neurons (Bishop et al., 2018; Bishop et al., 2015; Hwang, Fotuhi,
566 Bredt, Cunningham, & Snyder, 1993) while Kv2.2 is less broadly expressed (Bishop et al., 2015;
567 Hermanstyne et al., 2010; Hwang, Glatt, Bredt, Yellen, & Snyder, 1992; Johnston et al., 2008; Kihira et
568 al., 2010). In contrast to this, we find Kv2.2 expressed in at least 90% of mouse DRG neurons. We also
569 identify that Kv2.2 is enriched in the DRG relative to neurons in the spinal cord, suggesting that
570 abundant Kv2.2 protein expression is a distinct feature of DRG neuron physiology. In central neurons,
571 Kv2 channel clusters are typically evenly distributed across neuron somata (Bishop et al., 2015; Kihira et
572 al., 2010; Muennich & Fyffe, 2004) and asymmetric subcellular localization of Kv2 clusters on neuron
573 somata has to our knowledge not been described. We find that Kv2 channels are enriched at the plasma
574 membrane in a subcellular region near the stem axon of some DRG neurons. Differences in Kv2
575 localization between central and somatosensory neurons could arise from differences in the
576 extracellular environment surrounding DRG neuron somata. In central neurons, Kv2 channel clusters are
577 reported at cholinergic C-terminal synaptic sites, S-type synapses, and apposed to astrocytic end feet
578 (Du et al., 1998; Muennich & Fyffe, 2004). However, synapses have not been reported in the DRG and
579 DRG neurons are surrounded by satellite glia instead of astrocytes (Matsuda et al., 2005). Further
580 studies could investigate if Kv2 clusters are localized to extracellular structures in the DRG. Kv2.2 has
581 been identified in juxtaparanodes but not paranodes of axons in the osseous spiral lamina of the cochlea
582 (Kim & Rutherford, 2016) and previous work has also identified that Kv2.1 channels are necessary for
583 enabling ER Ca2+ uptake during electrical activity in both the soma and axon (Panzera et al., 2022). To
584 our knowledge, Kv2.2 immunofluorescence has not been previously reported in distal axons in the brain,
585 spinal cord or DRG. Our results indicate that Kv2.2 channels are present in myelinated and unmyelinated
586 axons of DRG neurons. The mechanism of Kv2.2 protein trafficking to the axon is unknown. Kv2.1
587 channels are trafficked to the axon initial segment through a distinct secretory pathway (Jensen et al.,

588 2017) allowing neurons to regulate precise compartment specific localization of Kv2.1 protein. A similar
589 mechanism for Kv2.2 localization in DRG axons could allow neurons to independently control Kv2.2
590 protein expression in the neuron soma and axon. The subcellular distribution of Kv2.1 and Kv2.2
591 subunits in DRG neurons suggests they could each distinctly modulate electrical signals. We note that
592 our observations could not distinguish whether immunofluorescence in DRG axons could represent
593 intracellular trafficking vesicles of Kv2.2 proteins, or whether axonal Kv2.2 is on the membrane surface
594 where it could modulate electrical signals.
595
596 Kv2 channels in DRG neurons may play important roles in somatosensation and nociception. Kv2
597 conductances can modulate action potential repolarization, afterhyperpolarization and repetitive firing
598 (Liu & Bean, 2014; Zheng et al., 2019). Kv2 conductances modulate electrical transmission in rat DRG
599 neurons (Tsantoulas et al., 2014). Knockdown of Kv2.1 increases hypersensitivity to painful stimuli and
600 regulation of Kv2.1 protein expression through the epigenetic factor Cdyl modulates neuronal
601 excitability and nociception (Sun et al., 2022). Consistent with these studies, our results show that Kv2
602 channels are localized to DRG neuron axons, where they could potentially influence electrical
603 transmission.
604
605 Regulatory pore-forming subunits of the Kv5, Kv6, Kv8, and Kv9 "silent subunit" families obligately
606 assemble into heteromeric channels with Kv2 subunits (Bocksteins, 2016) and have been implicated in
607 nociception. Women with decreased sensitivity to labor pain were identified to have a mutation in the
608 Kv6.4 silent subunit that disrupts Kv2.1/Kv6.4 heteromer expression and is proposed to modulate
609 nociceptor signaling (Lee et al., 2020). Downregulation of the Kv9.1 silent subunit after axotomy evokes
610 hyperexcitability of DRG neurons (Tsantoulas et al., 2012). While both Kv2 channels are broadly
611 expressed in DRG neurons, transcript levels of silent subunits in mice and humans show much more

612 neuron subtype specificity (Tavares-Ferreira et al., 2022; Zheng et al., 2019), raising the possibility of
613 molecularly distinct Kv2-containing channels in somatosensory neuron subtypes.
614
615 Previous studies have identified that voltage gated ion channel expression can be substantially different
616 between mice and human DRG, notably, in the expression of Nav1.7 (Shiers et al., 2020). However, we
617 find expression of Kv2 channels to be similar in mouse and human DRG. An overall similarity is
618 supported by the presence of detectable Kv2 channels in most neurons, consistent with transcriptomics
619 data from both mice and humans (Tavares-Ferreira et al., 2022; Zheng et al., 2019). The subcellular
620 localization of Kv2 channels also appears similar between mice and humans. These similarities include
621 enrichment of Kv2 channels at the outer edge of neurons, Kv2 clusters on the neuron soma as well as
622 presence of Kv2.1 and Kv2.2 on DRG neuron axons. These similarities suggest that the functional roles of
623 Kv2 channels could be similar in both mouse and human DRG neurons.
624
625 Overall, we find attributes of Kv2 channel localization in somatosensory neurons that could point to
626 their functional roles in sensory information processing. The broad expression of Kv2.2 among DRG
627 neuron types and expansive axonal localization of Kv2.2 suggest a key role for this channel in the
628 somatosensory nervous system. The specialized divergence of Kv2.1 and Kv2.2 suggest the functional
629 roles of Kv2 subtypes in DRG neurons are overlapping yet distinct.

630 **REFERENCES**

631

632 Bishop, H. I., Cobb, M. M., Kirmiz, M., Parajuli, L. K., Mandikian, D., Philp, A. M., . . . Trimmer, J.
633 S. (2018). Kv2 ion channels determine the expression and localization of the associated
634 AMIGO-1 cell adhesion molecule in adult brain neurons. *Front Mol Neurosci, 11*, 1.
635 doi:10.3389/fnmol.2018.00001
636 Bishop, H. I., Guan, D., Bocksteins, E., Parajuli, L. K., Murray, K. D., Cobb, M. M., . . . Trimmer, J.
637 S. (2015). Distinct cell- and layer-specific expression patterns and independent
638 regulation of Kv2 channel subtypes in cortical pyramidal neurons. *J Neurosci, 35*(44),
639 14922-14942. doi:10.1523/jneurosci.1897-15.2015
640 Blaine, J. T., & Ribera, A. B. (1998). Heteromultimeric potassium channels formed by members
641 of the Kv2 subfamily. *J Neurosci, 18*(23), 9585-9593. doi:10.1523/jneurosci.18-23-
642 09585.1998
643 Bocksteins, E. (2016). Kv5, Kv6, Kv8, and Kv9 subunits: No simple silent bystanders. *J Gen*
644 *Physiol, 147*(2), 105-125. doi:10.1085/jgp.201511507
645 Bocksteins, E., Raes, A. L., Van de Vijver, G., Bruyns, T., Van Bogaert, P. P., & Snyders, D. J.
646 (2009). Kv2.1 and silent Kv subunits underlie the delayed rectifier K+ current in cultured
647 small mouse DRG neurons. *Am J Physiol Cell Physiol, 296*(6), C1271-1278.
648 doi:10.1152/ajpcell.00088.2009
649 Cho, W. G., & Valtschanoff, J. G. (2008). Vanilloid receptor TRPV1-positive sensory afferents in
650 the mouse ankle and knee joints. *Brain Res., 1219*, 59-65.
651 doi:https://doi.org/10.1016/j.brainres.2008.04.043
652 Coggeshall, R. E. (1992). A consideration of neural counting methods. *Trends Neurosci, 15*(1), 9-
653 13. doi:10.1016/0166-2236(92)90339-a
654 Coggeshall, R. E., & Lekan, H. A. (1996). Methods for determining numbers of cells and
655 synapses: a case for more uniform standards of review. *J Comp Neurol, 364*(1), 6-15.
656 doi:10.1002/(SICI)1096-9861(19960101)364:1<6::AID-CNE2>3.0.CO;2-9
657 Cotella, D., Hernandez-Enriquez, B., Wu, X., Li, R., Pan, Z., Leveille, J., . . . Sesti, F. (2012). Toxic
658 role of K+ channel oxidation in mammalian brain. *J Neurosci, 32*(12), 4133-4144.
659 doi:10.1523/jneurosci.6153-11.2012
660 Dirajlal, S., Pauers, L. E., & Stucky, C. L. (2003). Differential response properties of IB(4)-positive
661 and -negative unmyelinated sensory neurons to protons and capsaicin. *J Neurophysiol,*
662 *89*(1), 513-524. doi:10.1152/jn.00371.2002
663 Dong, X., Han, S., Zylka, M. J., Simon, M. I., & Anderson, D. J. (2001). A diverse family of GPCRs
664 expressed in specific subsets of nociceptive sensory neurons. *Cell, 106*(5), 619-632.
665 doi:10.1016/s0092-8674(01)00483-4
666 Du, J., Tao-Cheng, J. H., Zerfas, P., & McBain, C. J. (1998). The K+ channel, Kv2.1, is apposed to
667 astrocytic processes and is associated with inhibitory postsynaptic membranes in
668 hippocampal and cortical principal neurons and inhibitory interneurons. *Neuroscience,*
669 *84*(1), 37-48. doi:https://doi.org/10.1016/S0306-4522(97)00519-8
670 Einheber, S., Zanazzi, G., Ching, W., Scherer, S., Milner, T. A., Peles, E., & Salzer, J. L. (1997). The
671 axonal membrane protein Caspr, a homologue of neurexin IV, is a component of the

672 septate-like paranodal junctions that assemble during myelination. *J Cell Biol, 139*(6),
673 1495-1506. doi:10.1083/jcb.139.6.1495
674 Fletcher, E. V., Simon, C. M., Pagiazitis, J. G., Chalif, J. I., Vukojicic, A., Drobac, E., . . . Mentis, G.
675 Z. (2017). Reduced sensory synaptic excitation impairs motor neuron function via Kv2.1
676 in spinal muscular atrophy. *Nat Neurosci, 20*(7), 905-916. doi:10.1038/nn.4561
677 Gravagna, N. G., Knoeckel, C. S., Taylor, A. D., Hultgren, B. A., & Ribera, A. B. (2008). Localization
678 of Kv2.2 protein in Xenopus laevis embryos and tadpoles. *J Comp Neurol, 510*(5), 508-
679 524. doi:10.1002/cne.21804
680 Ha, H. (1970). Axonal bifurcation in the dorsal root ganglion of the cat: a light and electron
681 microscopic study. *J Comp Neurol, 140*(2), 227-240. doi:10.1002/cne.901400206
682 He, X. H., Zang, Y., Chen, X., Pang, R. P., Xu, J. T., Zhou, X., . . . Liu, X. G. (2010). TNF-α
683 contributes to up-regulation of Nav1.3 and Nav1.8 in DRG neurons following motor fiber
684 injury. *Pain, 151*(2), 266-279. doi:10.1016/j.pain.2010.06.005
685 Hermanstyne, T. O., Kihira, Y., Misono, K., Deitchler, A., Yanagawa, Y., & Misonou, H. (2010).
686 Immunolocalization of the voltage-gated potassium channel Kv2.2 in GABAergic neurons
687 in the basal forebrain of rats and mice. *J Comp Neurol, 518*(21), 4298-4310.
688 doi:10.1002/cne.22457
689 Hwang, P. M., Fotuhi, M., Bredt, D. S., Cunningham, A. M., & Snyder, S. H. (1993). Contrasting
690 immunohistochemical localizations in rat brain of two novel K+ channels of the Shab
691 subfamily. *J Neurosci, 13*(4), 1569-1576. doi:10.1523/jneurosci.13-04-01569.1993
692 Hwang, P. M., Glatt, C. E., Bredt, D. S., Yellen, G., & Snyder, S. H. (1992). A novel K+ channel with
693 unique localizations in mammalian brain: molecular cloning and characterization.
694 *Neuron, 8*(3), 473-481. doi:10.1016/0896-6273(92)90275-i
695 Irie, T. (2021). Essential role of somatic Kv2 channels in high-frequency firing in cartwheel cells
696 of the dorsal cochlear nucleus. *eNeuro, 8*(3). doi:10.1523/eneuro.0515-20.2021
697 Jensen, C. S., Watanabe, S., Stas, J. I., Klaphaak, J., Yamane, A., Schmitt, N., . . . Misonou, H.
698 (2017). Trafficking of Kv2.1 channels to the axon initial segment by a novel
699 nonconventional secretory pathway. *J Neurosci, 37*(48), 11523-11536.
700 doi:10.1523/jneurosci.3510-16.2017
701 Johnson, B., Leek, A. N., Sole, L., Maverick, E. E., Levine, T. P., & Tamkun, M. M. (2018). Kv2
702 potassium channels form endoplasmic reticulum/plasma membrane junctions via
703 interaction with VAPA and VAPB. *Proc Natl Acad Sci U S A, 115*(31), E7331-e7340.
704 doi:10.1073/pnas.1805757115
705 Johnston, J., Griffin, S. J., Baker, C., Skrzypiec, A., Chernova, T., & Forsythe, I. D. (2008). Initial
706 segment Kv2.2 channels mediate a slow delayed rectifier and maintain high frequency
707 action potential firing in medial nucleus of the trapezoid body neurons. *J Physiol,*
708 *586*(14), 3493-3509. doi:10.1113/jphysiol.2008.153734
709 Kihira, Y., Hermanstyne, T. O., & Misonou, H. (2010). Formation of heteromeric Kv2 channels in
710 mammalian brain neurons. *J Biol Chem, 285*(20), 15048-15055.
711 doi:10.1074/jbc.M109.074260
712 Kim, K. X., & Rutherford, M. A. (2016). Maturation of NaV and Kv channel topographies in the
713 auditory nerve spike initiator before and after developmental onset of hearing function.
714 *J Neurosci, 36*(7), 2111-2118. doi:10.1523/jneurosci.3437-15.2016

King, A. N., Manning, C. F., & Trimmer, J. S. (2014). A unique ion channel clustering domain on the axon initial segment of mammalian neurons. *J Comp Neurol, 522*(11), 2594-2608. doi:10.1002/cne.23551

Kirmiz, M., Vierra, N. C., Palacio, S., & Trimmer, J. S. (2018). Identification of VAPA and VAPB as Kv2 channel-interacting proteins defining endoplasmic reticulum-plasma membrane junctions in mammalian brain neurons. *J Neurosci*. doi:10.1523/jneurosci.0893-18.2018

Lee, M. C., Nahorski, M. S., Hockley, J. R. F., Lu, V. B., Ison, G., Pattison, L. A., . . . Woods, C. G. (2020). Human labor pain is influenced by the voltage-gated potassium channel Kv 6.4 subunit. *Cell Rep, 32*(3), 107941. doi:10.1016/j.celrep.2020.107941

Legland, D., Arganda-Carreras, I., & Andrey, P. (2016). MorphoLibJ: integrated library and plugins for mathematical morphology with ImageJ. *Bioinformatics, 32*(22), 3532-3534. doi:10.1093/bioinformatics/btw413

Li, X. N., Herrington, J., Petrov, A., Ge, L., Eiermann, G., Xiong, Y., . . . Zhou, Y. P. (2013). The role of voltage-gated potassium channels Kv2.1 and Kv2.2 in the regulation of insulin and somatostatin release from pancreatic islets. *J Pharmacol Exp Ther, 344*(2), 407-416. doi:10.1124/jpet.112.199083

Lim, S. T., Antonucci, D. E., Scannevin, R. H., & Trimmer, J. S. (2000). A novel targeting signal for proximal clustering of the Kv2.1 K+ channel in hippocampal neurons. *Neuron, 25*(2), 385-397. doi:10.1016/s0896-6273(00)80902-2

Liu, P. W., & Bean, B. P. (2014). Kv2 channel regulation of action potential repolarization and firing patterns in superior cervical ganglion neurons and hippocampal CA1 pyramidal neurons. *J Neurosci, 34*(14), 4991-5002. doi:10.1523/jneurosci.1925-13.2014

Matsuda, S., Kobayashi, N., Terashita, T., Shimokawa, T., Shigemoto, K., Mominoki, K., . . . Fujiwara, T. (2005). Phylogenetic investigation of Dogiel's pericellular nests and Cajal's initial glomeruli in the dorsal root ganglion. *J Comp Neurol, 491*(3), 234-245. doi:10.1002/cne.20713

Misonou, H., Mohapatra, D. P., Menegola, M., & Trimmer, J. S. (2005). Calcium- and metabolic state-dependent modulation of the voltage-dependent Kv2.1 channel regulates neuronal excitability in response to ischemia. *J Neurosci, 25*(48), 11184-11193. doi:10.1523/jneurosci.3370-05.2005

Muennich, E. A., & Fyffe, R. E. (2004). Focal aggregation of voltage-gated, Kv2.1 subunit-containing, potassium channels at synaptic sites in rat spinal motoneurones. *J Physiol, 554*(Pt 3), 673-685. doi:10.1113/jphysiol.2003.056192

Newkirk, G. S., Guan, D., Dembrow, N., Armstrong, W. E., Foehring, R. C., & Spain, W. J. (2022). Kv2.1 potassium channels regulate repetitive burst firing in extratelencephalic neocortical pyramidal neurons. *Cereb Cortex, 32*(5), 1055-1076. doi:10.1093/cercor/bhab266

Panzera, L. C., Johnson, B., Quinn, J. A., Cho, I. H., Tamkun, M. M., & Hoppa, M. B. (2022). Activity-dependent endoplasmic reticulum Ca(2+) uptake depends on Kv2.1-mediated endoplasmic reticulum/plasma membrane junctions to promote synaptic transmission. *Proc Natl Acad Sci U S A, 119*(30), e2117135119. doi:10.1073/pnas.2117135119

Rasband, M. N., Trimmer, J. S., Schwarz, T. L., Levinson, S. R., Ellisman, M. H., Schachner, M., & Shrager, P. (1998). Potassium channel distribution, clustering, and function in

remyelinating rat axons. *J Neurosci, 18*(1), 36-47. doi:10.1523/jneurosci.18-01-00036.1998

Regnier, G., Bocksteins, E., Van de Vijver, G., Snyders, D. J., & van Bogaert, P. P. (2016). The contribution of Kv2.2-mediated currents decreases during the postnatal development of mouse dorsal root ganglion neurons. *Physiol Rep, 4*(6). doi:10.14814/phy2.12731

Romer, S. H., Dominguez, K. M., Gelpi, M. W., Deardorff, A. S., Tracy, R. C., & Fyffe, R. E. W. (2014). Redistribution of Kv2.1 ion channels on spinal motoneurons following peripheral nerve injury. *Brain research, 1547*, 1-15. doi:10.1016/j.brainres.2013.12.012

Sarmiere, P. D., Weigle, C. M., & Tamkun, M. M. (2008). The Kv2.1 K+ channel targets to the axon initial segment of hippocampal and cortical neurons in culture and in situ. *BMC Neurosci, 9*, 112. doi:10.1186/1471-2202-9-112

Scannevin, R. H., Murakoshi, H., Rhodes, K. J., & Trimmer, J. S. (1996). Identification of a cytoplasmic domain important in the polarized expression and clustering of the Kv2.1 K+ channel. *J Cell Biol, 135*(6 Pt 1), 1619-1632. doi:10.1083/jcb.135.6.1619

Schindelin, J., Arganda-Carreras, I., Frise, E., Kaynig, V., Longair, M., Pietzsch, T., . . . Cardona, A. (2012). Fiji: an open-source platform for biological-image analysis. *Nat Methods, 9*(7), 676-682. doi:10.1038/nmeth.2019

Scott, B., Leu, J., & Cinader, B. (1988). Effects of aging on neuronal electrical membrane properties. *Mech Ageing Dev, 44*(3), 203-214. doi:10.1016/0047-6374(88)90022-x

Shields, S. D., Ahn, H. S., Yang, Y., Han, C., Seal, R. P., Wood, J. N., . . . Dib-Hajj, S. D. (2012). Nav1.8 expression is not restricted to nociceptors in mouse peripheral nervous system. *Pain, 153*(10), 2017-2030. doi:10.1016/j.pain.2012.04.022

Shiers, S., Klein, R. M., & Price, T. J. (2020). Quantitative differences in neuronal subpopulations between mouse and human dorsal root ganglia demonstrated with RNAscope in situ hybridization. *Pain, 161*(10), 2410-2424. doi:10.1097/j.pain.0000000000001973

Shiers, S., Sankaranarayanan, I., Jeevakumar, V., Cervantes, A., Reese, J. C., & Price, T. J. (2021). Convergence of peptidergic and non-peptidergic protein markers in the human dorsal root ganglion and spinal dorsal horn. *J Comp Neurol, 529*(10), 2771-2788. doi:10.1002/cne.25122

Sun, Z. W., Waybright, J. M., Beldar, S., Chen, L., Foley, C. A., Norris-Drouin, J. L., . . . Wang, Y. (2022). Cdyl deficiency brakes neuronal excitability and nociception through promoting Kcnb1 transcription in peripheral sensory neurons. *Adv Sci (Weinh), 9*(10), e2104317. doi:10.1002/advs.202104317

Tavares-Ferreira, D., Shiers, S., Ray, P. R., Wangzhou, A., Jeevakumar, V., Sankaranarayanan, I., . . . Price, T. J. (2022). Spatial transcriptomics of dorsal root ganglia identifies molecular signatures of human nociceptors. *Sci Transl Med, 14*(632), eabj8186. doi:10.1126/scitranslmed.abj8186

Thapa, P., Stewart, R., Sepela, R. J., Vivas, O., Parajuli, L. K., Lillya, M., . . . Sack, J. T. (2021). EVAP: A two-photon imaging tool to study conformational changes in endogenous Kv2 channels in live tissues. *J Gen Physiol, 153*(11). doi:10.1085/jgp.202012858

Trimmer, J. S. (1991). Immunological identification and characterization of a delayed rectifier K+ channel polypeptide in rat brain. *Proc Natl Acad Sci U S A, 88*(23), 10764-10768. doi:10.1073/pnas.88.23.10764

801 Tsantoulas, C., Zhu, L., Shaifta, Y., Grist, J., Ward, J. P., Raouf, R., . . . McMahon, S. B. (2012).
802 Sensory neuron downregulation of the Kv9.1 potassium channel subunit mediates
803 neuropathic pain following nerve injury. *J Neurosci, 32*(48), 17502-17513.
804 doi:10.1523/jneurosci.3561-12.2012
805 Tsantoulas, C., Zhu, L., Yip, P., Grist, J., Michael, G. J., & McMahon, S. B. (2014). Kv2 dysfunction
806 after peripheral axotomy enhances sensory neuron responsiveness to sustained input.
807 *Exp Neurol, 251*, 115-126. doi:10.1016/j.expneurol.2013.11.011
808 Usoskin, D., Furlan, A., Islam, S., Abdo, H., Lönnerberg, P., Lou, D., . . . Ernfors, P. (2015).
809 Unbiased classification of sensory neuron types by large-scale single-cell RNA
810 sequencing. *Nat Neurosci, 18*(1), 145-153. doi:10.1038/nn.3881
811 Valtcheva, M. V., Copits, B. A., Davidson, S., Sheahan, T. D., Pullen, M. Y., McCall, J. G., . . .
812 Gereau, R. W. t. (2016). Surgical extraction of human dorsal root ganglia from organ
813 donors and preparation of primary sensory neuron cultures. *Nat Protoc, 11*(10), 1877-
814 1888. doi:10.1038/nprot.2016.111
815 Vierra, N. C., O'Dwyer, S. C., Matsumoto, C., Santana, L. F., & Trimmer, J. S. (2021). Regulation
816 of neuronal excitation-transcription coupling by Kv2.1-induced clustering of somatic L-
817 type Ca(2+) channels at ER-PM junctions. *Proc Natl Acad Sci U S A, 118*(46).
818 doi:10.1073/pnas.2110094118
819 Vullhorst, D., Mitchell, R. M., Keating, C., Roychowdhury, S., Karavanova, I., Tao-Cheng, J. H., &
820 Buonanno, A. (2015). A negative feedback loop controls NMDA receptor function in
821 cortical interneurons via neuregulin 2/ErbB4 signalling. *Nat Commun, 6*, 7222.
822 doi:10.1038/ncomms8222
823 Wang, H., & Zylka, M. J. (2009). Mrgprd-expressing polymodal nociceptive neurons innervate
824 most known classes of substantia gelatinosa neurons. *J Neurosci, 29*(42), 13202-13209.
825 doi:10.1523/jneurosci.3248-09.2009
826 Wangzhou, A., McIlvried, L. A., Paige, C., Barragan-Iglesias, P., Shiers, S., Ahmad, A., . . . Price, T.
827 J. (2020). Pharmacological target-focused transcriptomic analysis of native vs cultured
828 human and mouse dorsal root ganglia. *Pain, 161*(7), 1497-1517.
829 doi:10.1097/j.pain.0000000000001866
830 Zheng, Y., Liu, P., Bai, L., Trimmer, J. S., Bean, B. P., & Ginty, D. D. (2019). Deep sequencing of
831 somatosensory neurons reveals molecular determinants of intrinsic physiological
832 properties. *Neuron, 103*(4), 598-616.e597. doi:10.1016/j.neuron.2019.05.039
833

FIGURES AND FIGURE LEGENDS

Figure 1

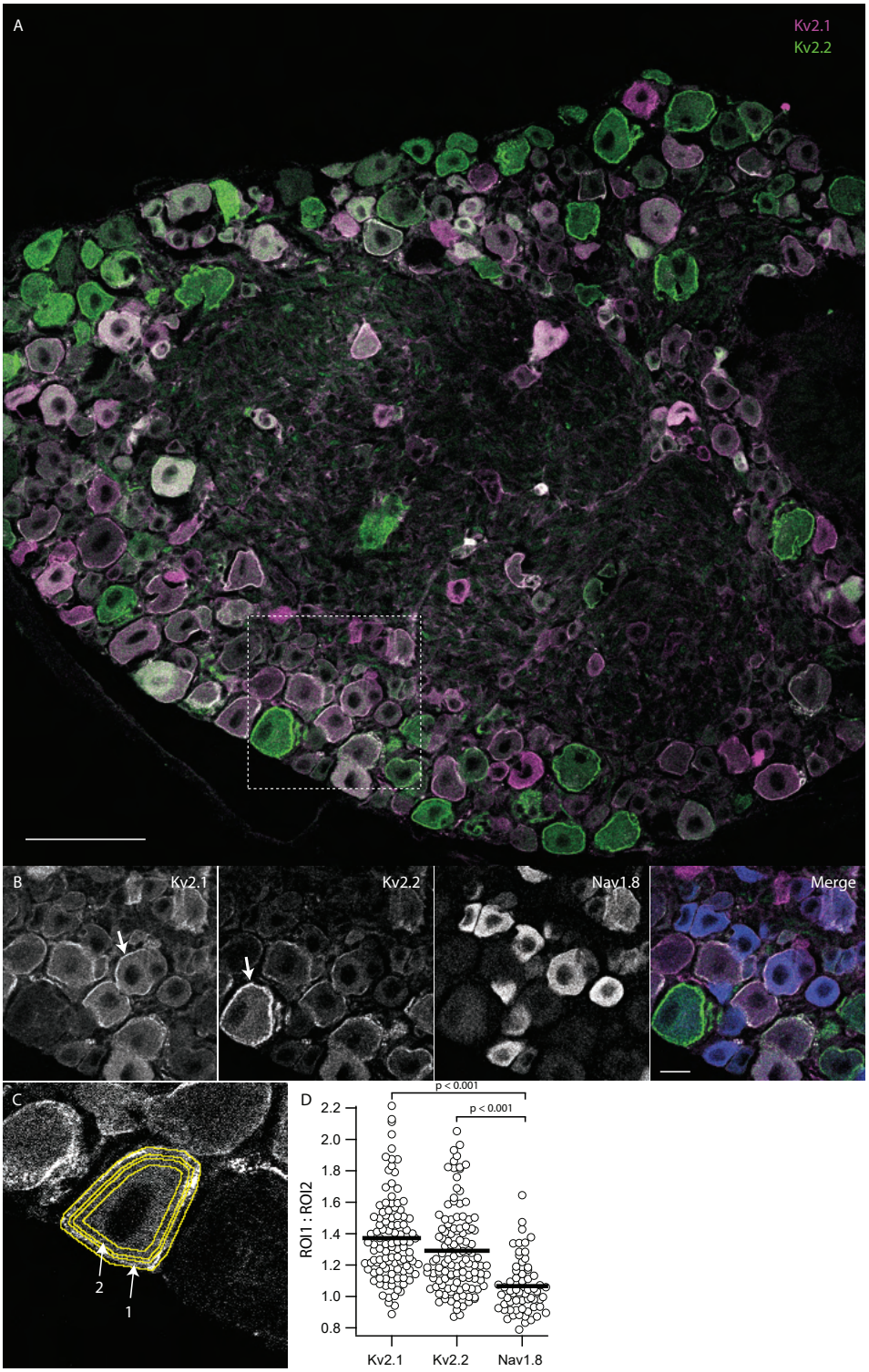

837 **Figure 1 legend**

838 Kv2.1 and Kv2.2 protein are enriched at the outer edge of DRG neuron somas relative to
839 Nav1.8. Lumbar DRG section from an 11 week old male mouse labeled with antibodies which
840 target Kv2.1, Kv2.2 or Nav1.8. ***A***, Anti-Kv2.1 (magenta) and anti-Kv2.2 (green)
841 immunofluorescence in a lumbar DRG section. Scale bar is 100 µm. ***B***, Anti-Kv2.1, anti-Kv2.2 and
842 anti-Nav1.8 immunofluorescence from box shown in A. Arrows indicate prominent localization
843 of anti-Kv2 immunofluorescence at the edge of DRG neuron somas. In merge image anti-Kv2.1,
844 anti-Kv2.2 and anti-Nav1.8 immunofluorescence is magenta, green and blue respectively. Scale
845 bar is 20 µm. ***C***, Representative ROIs that encompass the outer edge of DRG neurons (arrow 1)
846 and the region just inside the outer edge (arrow 2). ***D***, Ratio of anti-Kv2.1, anti-Kv2.2 or anti-
847 Nav1.8 immunofluorescence from outer and inner ROIs for individual neurons from image in A.
848 Bars represent mean. One-way ANOVA $p < 0.001$. p values in figure represent post hoc Tukey's
849 test. N = 1 mouse, n = 124 neurons. Detailed information on mouse used can be found in table
850 1.

Figure 2

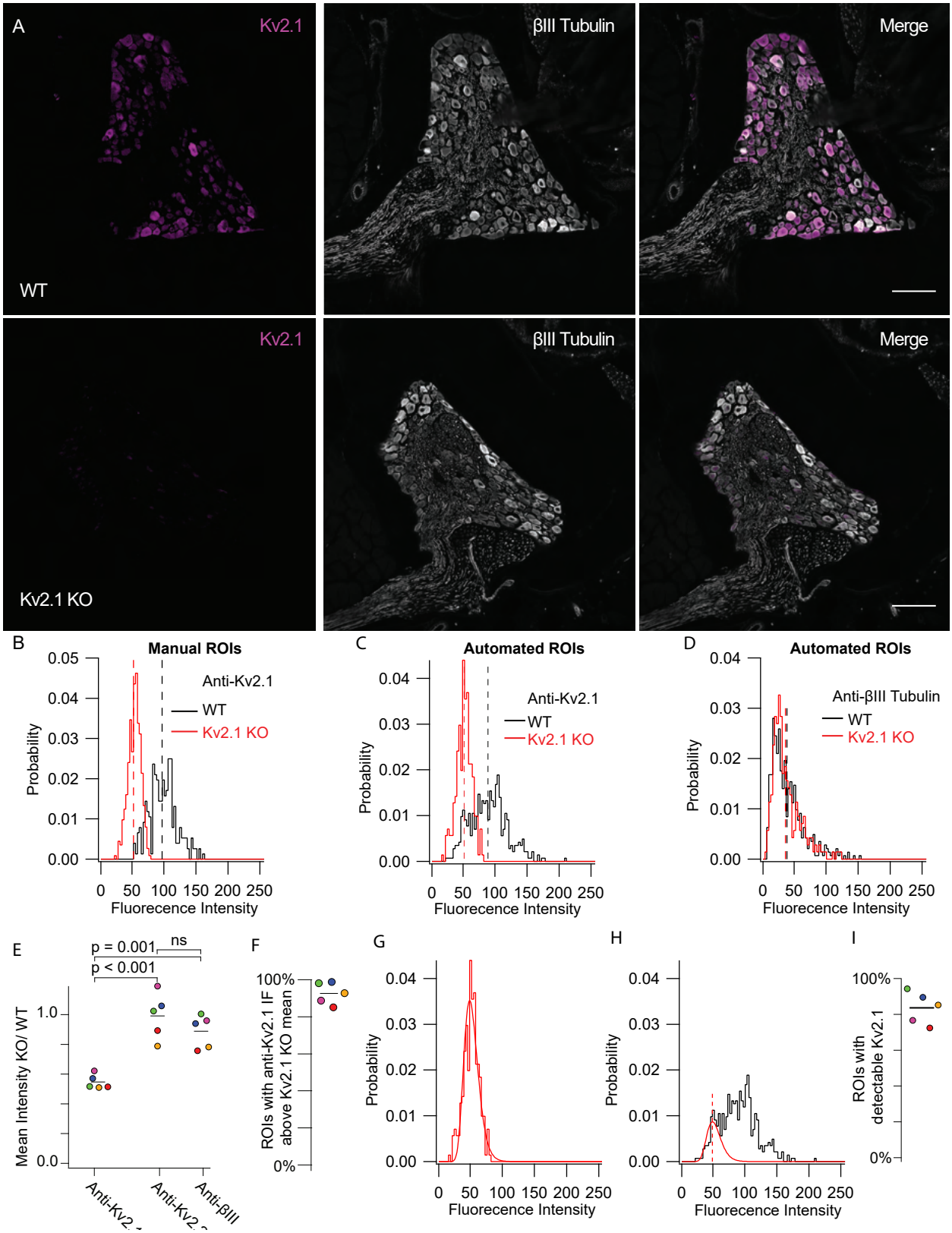
A
Kv2.1
βIII Tubulin
Merge
WT
Kv2.1 KO
B
Manual ROIs
Anti-Kv2.1
WT
Kv2.1 KO
Probability
Fluorecence Intensity
C
Automated ROIs
D
Anti-βIII Tubulin
E
p = 0.001
ns
p < 0.001
Mean Intensity KO/ WT
F
ROIs with anti-Kv2.1 IF above Kv2.1 KO mean
G
H
I
ROIs with detectable Kv2.1

853 **Figure 2 legend**

854 Kv2.1 protein is detectable in mouse DRG neurons. ***A***, WT (top) and Kv2.1 KO (bottom) DRG
855 sections taken from 7 week old female mice from the 13th thoracic DRG immunolabeled for
856 Kv2.1 (magenta) and BIII tubulin (white). Images were taken with identical imaging settings and
857 are set to the same brightness and contrast. Scale bars are 100 µm. ***B***, Distribution of
858 fluorescence intensity from manual analysis of WT (black) and Kv2.1 KO (red) neurons. Dotted
859 lines represent mean. Data represent fluorescence intensity of 254 WT profiles from 10 DRG
860 sections from 1 mouse or 375 Kv2.1 KO profiles from 5 DRG sections from 1 mouse. Images
861 shown in A represent one section from WT and Kv2.1 KO mice used in this data set. ***C***,
862 Distribution of fluorescence intensity from automated analysis of the same data set shown in B.
863 Dotted lines represent mean. Data represent fluorescence intensity of 476 WT or 576 Kv2.1 KO
864 profiles selected by automated analysis method. ***D***, Distribution of BIII tubulin fluorescence
865 intensity from the same WT (black) and Kv2.1 KO (red) profiles shown in C. Dotted lines
866 represent mean. ***E***, Mean fluorescence intensity of Kv2.1 KO neurons normalized to WT neurons
867 labeled with anti-Kv2.1, anti-Kv2.2 and anti-BIII tubulin antibodies. Each point represents one
868 Kv2.1 KO mouse normalized to one age and sex matched WT mouse which was stained
869 simultaneously and imaged with identical microscopy settings. The color of each point
870 represents the same mouse and purple points represent data from the mouse whose DRG
871 immunofluorescence data are shown in A, B, C and D. one-way ANOVA $p < 0.001$. p values in
872 figure represent post hoc Tukey's test. ***F***, Percentage of ROIs with anti-Kv2.1
873 immunofluorescence above the mean immunofluorescence of 5 mice (1 female and 4 male).
874 Point colors correspond to the WT mice analyzed in E. All mice were compared to age and sex

875 matched Kv2.1 KO mice. N = 5 WT and 5 Kv2.1 KO mice. ***G***, Kv2.1 KO data shown in B fit with a
876 log normal distribution (red fit). ***H***, WT data shown in B fit with the Kv2.1 KO distribution (red
877 fit) where width and mean were constrained to the Kv2.1 KO distribution and amplitude was
878 unconstrained (equation 1). Red dotted line represents the mean of the Kv2.1 KO distribution.
879 Only WT data to the left of red dotted line was used for the fit. ***I***, Percentage of ROIs with
880 detectable Kv2.1 protein of 5 mice (1 female and 4 males). Point colors correspond to the WT
881 mice analyzed in E. All mice were compared to age and sex matched Kv2.1 KO mice. N = 5 WT
882 and 5 Kv2.1 KO mice. Detailed information on each mouse used can be found in table 1.
883

Figure 3

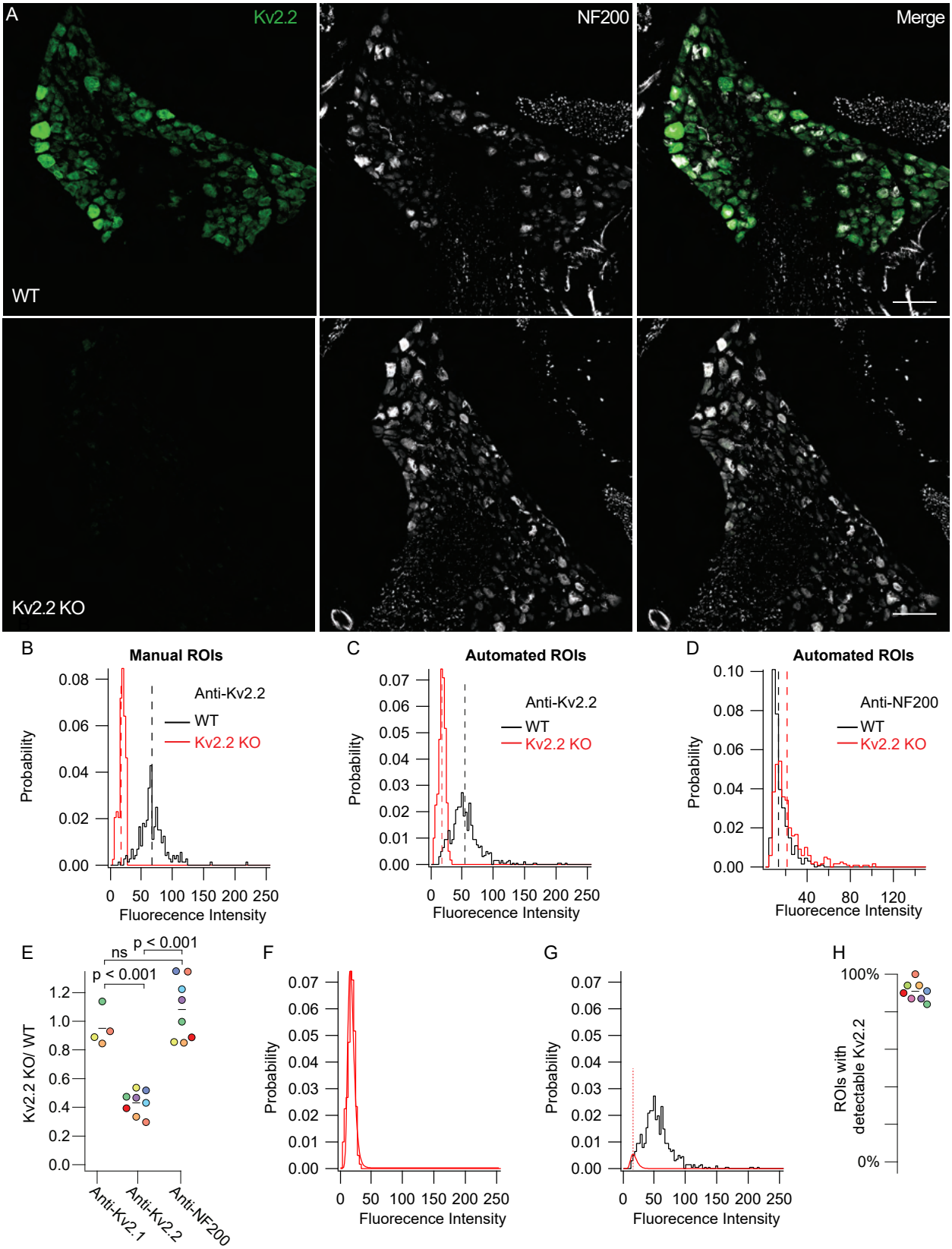
A
Kv2.2
NF200
Merge
WT
Kv2.2 KO
B
Manual ROIs
Anti-Kv2.2
WT
Kv2.2 KO
Probability
Fluorecence Intensity
C
Automated ROIs
Anti-Kv2.2
WT
Kv2.2 KO
Probability
Fluorecence Intensity
D
Automated ROIs
Anti-NF200
WT
Kv2.2 KO
Probability
Fluorecence Intensity
E
ns
p < 0.001
p < 0.001
Kv2.2 KO/ WT
Anti-Kv2.1
Anti-Kv2.2
Anti-NF200
F
Probability
Fluorecence Intensity
G
Probability
Fluorecence Intensity
H
ROIs with detectable Kv2.2
100%
0%

886 **Figure 3 legend**

887 Kv2.2 protein is detectable in mouse DRG neurons. ***A***, WT (top) and Kv2.2 KO (bottom) DRG
888 sections from the 13th thoracic DRG in 7 week old male mice immunolabeled for Kv2.2 (green)
889 and NF200 (white). Identical imaging and display settings. Scale bars are 100 µm. **B**,
890 Distribution of fluorescence intensities from manual analysis of WT (black) and Kv2.2 KO (red)
891 profiles. Dotted lines represent mean. Data represents fluorescence intensities from 241 WT
892 profiles from 11 DRG sections and 1 mouse or 130 Kv2.2 KO profiles from 6 DRG sections and 1
893 mouse. Images shown in A represent one section from WT and Kv2.1 KO mice used in this data
894 set. ***C***, Distribution of fluorescence intensity from automated analysis of the same data set
895 shown in B. Dotted lines represent mean. Data represent fluorescence intensity of 673 WT or
896 400 Kv2.2 KO profiles selected by automated analysis method. ***D***, Distribution of anti-NF200
897 immunofluorescence intensity from the same WT (black) and Kv2.2 KO (red) neurons shown in
898 B. Dotted lines represent mean. ***E***, Mean fluorescence intensity of Kv2.2 KO ROIs normalized to
899 WT neurons labeled with anti-Kv2.1, anti-Kv2.2 and anti-NF200 antibodies. Each point
900 represents one Kv2.2 KO mouse normalized to one age and sex matched WT mouse which was
901 stained simultaneously and imaged with identical microscopy settings. The color of each point
902 represents the same mouse and purple points represent data from the male mouse whose DRG
903 immunofluorescence data are shown in A, B and C. Missing points in anti-Kv2.1 column are
904 because some sections were not labeled with anti-Kv2.1 antibodies. one-way ANOVA $p < 0.001$.
905 p values in figure represent Tukey's post hoc test. ***F***, Kv2.2 KO data shown in B fit with a log
906 normal distribution (red fit). ***G***, WT data shown in B fit with the Kv2.2 KO distribution (red fit)
907 where width and mean were constrained to the Kv2.2 KO distribution and amplitude was

908 unconstrained (equation 1). Red dotted line represents the mean of the Kv2.2 KO distribution.

909 Only WT data to the left of red dotted line was used for the fit. ***H***, Percentage of ROIs with

910 detectable Kv2.2 protein of 8 mice (7 males and 1 female). Point colors correspond to the WT

911 mice analyzed in D. All mice were compared to age and sex matched Kv2.2 KO mice. N = 8 WT

912 and 8 Kv2.2 KO mice. Detailed information on each mouse used can be found in table 1.

913

Figure 4

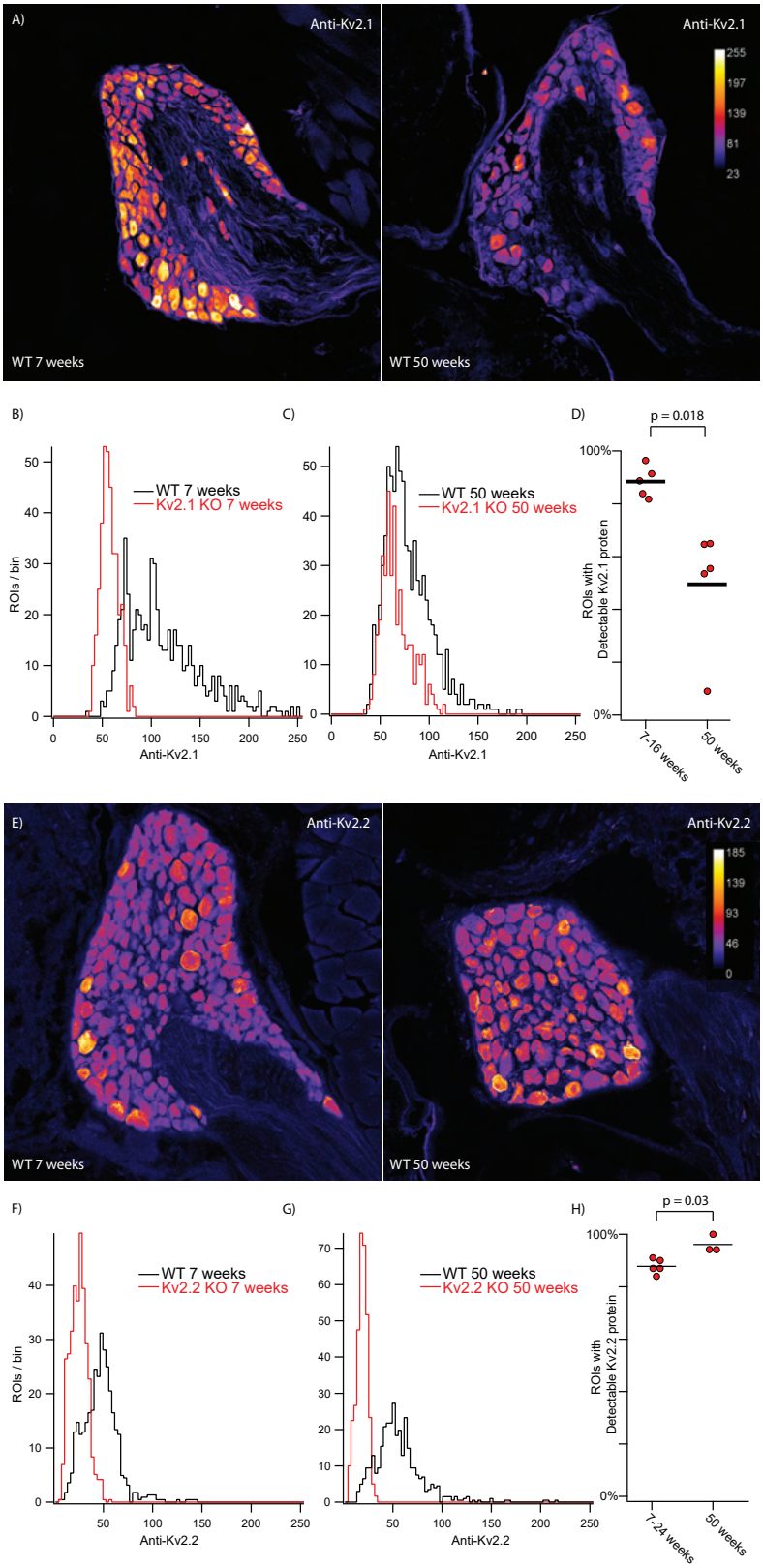
A)
Anti-Kv2.1
WT 7 weeks
Anti-Kv2.1
255
197
139
81
23
WT 50 weeks
B)
WT 7 weeks
Kv2.1 KO 7 weeks
ROIs / bin
Anti-Kv2.1
C)
WT 50 weeks
Kv2.1 KO 50 weeks
Anti-Kv2.1
D)
p = 0.018
100%
0%
ROIs with Detectable Kv2.1 protein
7-16 weeks
50 weeks
E)
Anti-Kv2.2
WT 7 weeks
Anti-Kv2.2
185
139
93
46
0
WT 50 weeks
F)
WT 7 weeks
Kv2.2 KO 7 weeks
ROIs / bin
Anti-Kv2.2
G)
WT 50 weeks
Kv2.2 KO 50 weeks
Anti-Kv2.2
H)
p = 0.03
100%
0%
ROIs with Detectable Kv2.2 protein
7-24 weeks
50 weeks

916 **Figure 4 legend**

917 Detectable Kv2.1 protein decreases in older mice while detectable Kv2.2 does not. ***A***, DRG
918 sections from the 13th thoracic DRG in 7 week (left) and 50 week (right) old mice
919 immunolabeled for Kv2.1. Vertical bar on right is pseudo coloring key for pixel intensity.
920 Identical imaging and display settings. Scale bars are 100 µm. ***B***, Distribution of fluorescence
921 intensities from 7 week old WT (black) and 7 week old Kv2.1 KO (red) ROIs generated by
922 automated method. 609 WT ROIs from 1 mouse. 367 Kv2.1 KO ROIs from 1 mouse. ***C***,
923 Distribution of fluorescence intensities from 50 week old WT (black) and 50 week old Kv2.1 KO
924 (red) ROIs. 793 WT ROIs from 1 mouse. 378 Kv2.1 KO ROIs from 1 mouse. ***D***, Percentage of ROIs
925 with detectable Kv2.1 protein in 7-16 week old and 50 week old mice. Data from 7-16 week old
926 mice is the same data in Figure 2. N = 4 mice 7 weeks old and 1 mouse 16 weeks old and N = 5
927 mice 50 weeks old. Detailed information on each mouse used can be found in table 1. ***E***, DRG
928 sections from the 13th thoracic DRG in 7 week (left) and 50 week (right) old mice
929 immunolabeled for Kv2.2. Vertical bar on right is pseudo coloring key for pixel intensity.
930 Identical imaging and display settings. Scale bars are 100 µm. ***F***, Distribution of fluorescence
931 intensities from 7 week old WT (black) and 7 week old Kv2.2 KO (red) ROIs generated by
932 automated method. 746 WT ROIs from 1 mouse. 717 Kv2.2 KO ROIs from 1 mouse. Data from
933 same mice shown in E. ***G***, Distribution of fluorescence intensities from 50 week old WT (black)
934 and 50 week old Kv2.2 KO (red) ROIs generated by automated method. 671 WT ROIs from 1
935 mouse. 398 Kv2.2 KO ROIs from 1 mouse. Data from same mice shown in E. ***H***, Percentage of
936 ROIs with detectable Kv2.2 protein in 7-24 week old and 50 week old mice. Data is the same
937 data from Figure 3 where mice were separated into a young group (7-24 weeks) and an old

938 group (50 weeks). N = 3 mice 7 weeks old, 1 mouse 24 weeks old and 1 mouse 25 weeks old. N

939 = 3 mice 50 weeks old. Detailed information on each mouse used can be found in table 1.

940

941 **Figure 5**

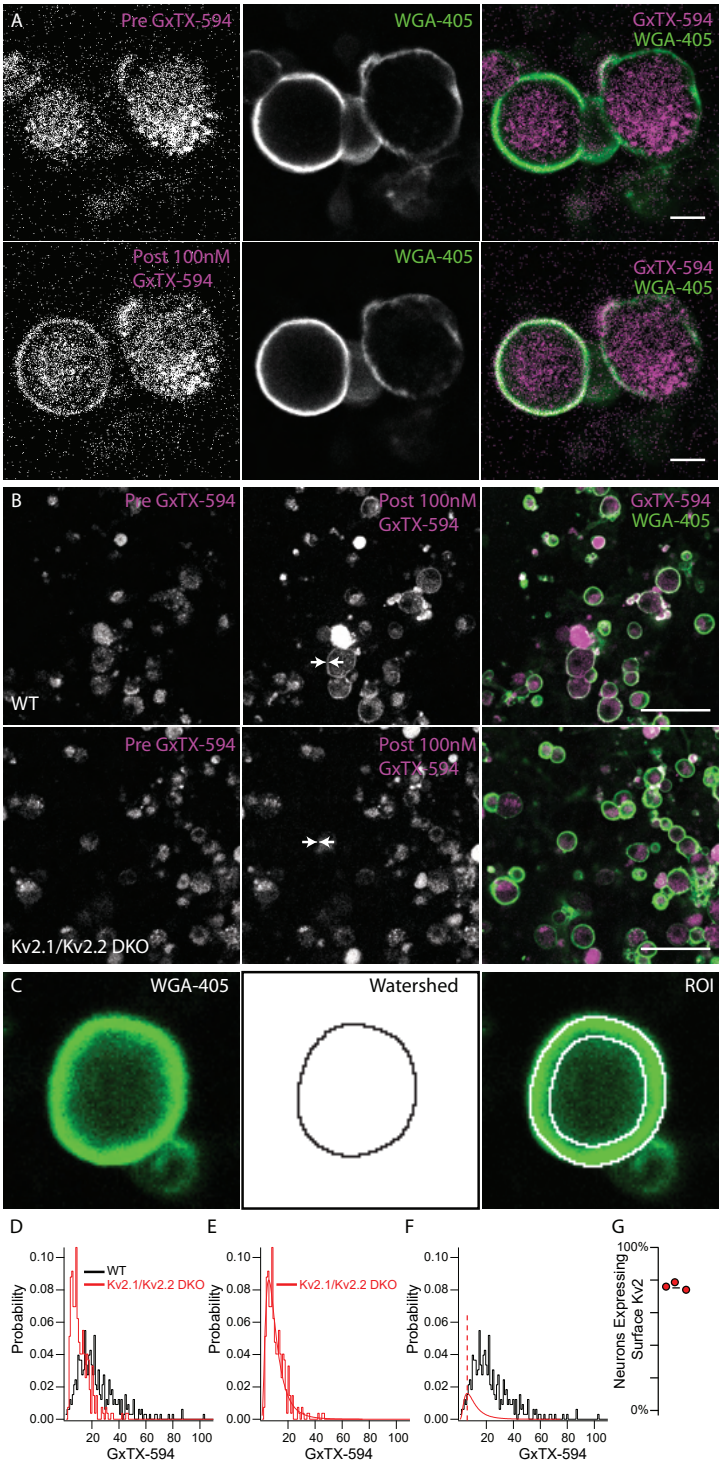

942

943 **Figure 5 legend**

944 Kv2 channels are expressed at the surface membrane of DRG neurons. ***A***, Fluorescence of live
945 dissociated DRG neurons excited at 594 nm before (top left) and after (bottom left) application
946 of 100 nM GxTX-594. Fluorescence from membrane marker WGA-405 before (top middle) and
947 after application of 100 nM GxTX-594 (bottom middle). Merge image shows 594 excitation
948 fluorescence (magenta) and 405 excitation fluorescence (green). Scale bar 20 µm. ***B***,
949 Dissociated DRG neurons from WT (top) and Kv2.1/Kv2.2 DKO (bottom) mice before and after
950 the application of GxTX-594, left panel and middle panel respectively. Arrows in middle panel
951 indicate location of surface membrane based on WGA-405 fluorescence. Right images are
952 merge of 594 excitation fluorescence (magenta) and 405 excitation fluorescence (green) after
953 application of 100 nM GxTX-594. Scale bars 100 µm. ***C***, Example of WGA-405 fluorescence (left)
954 used in watershed segmentation (middle) to generate annulus ROI (right) used to analyze
955 fluorescence intensity at the membrane. ***D***, Distribution of fluorescence intensity from WT
956 (black) and Kv2.1/Kv2.2 DKO (red) neurons. Data represents the fluorescence intensity of 326
957 WT neurons from 1 mouse or 271 Kv2.1/Kv2.2 DKO neurons from 1 mouse. DRG from all levels
958 of the spinal cord were pooled. ***E***, Kv2.1/Kv2.2 DKO data shown in D fit with a log normal
959 distribution (red fit). ***F***, WT data shown in D fit with the Kv2.1/Kv2.2 DKO distribution (red fit)
960 where width and mean were constrained to the Kv2.1/Kv2.2 DKO distribution and amplitude
961 was unconstrained (equation 1). Red dotted line represents the mean of the Kv2.1/Kv2.2 DKO
962 distribution. Only WT data to the left of red dotted line was used for the fit. ***G***, Percentage of
963 neurons with detectable surface Kv2 protein, from an experiment where one WT mouse was
964 compared to one DKO mouse and an identical experiment where two WT mice were compared

965 to one DKO mouse (N=3 WT mice N=2 Kv2.1/Kv2.2 DKO mice). N = 3 WT mice and N = 2 DKO

966 mice. Detailed information on each mouse used can be found in table 1.

967

968 **Figure 6**

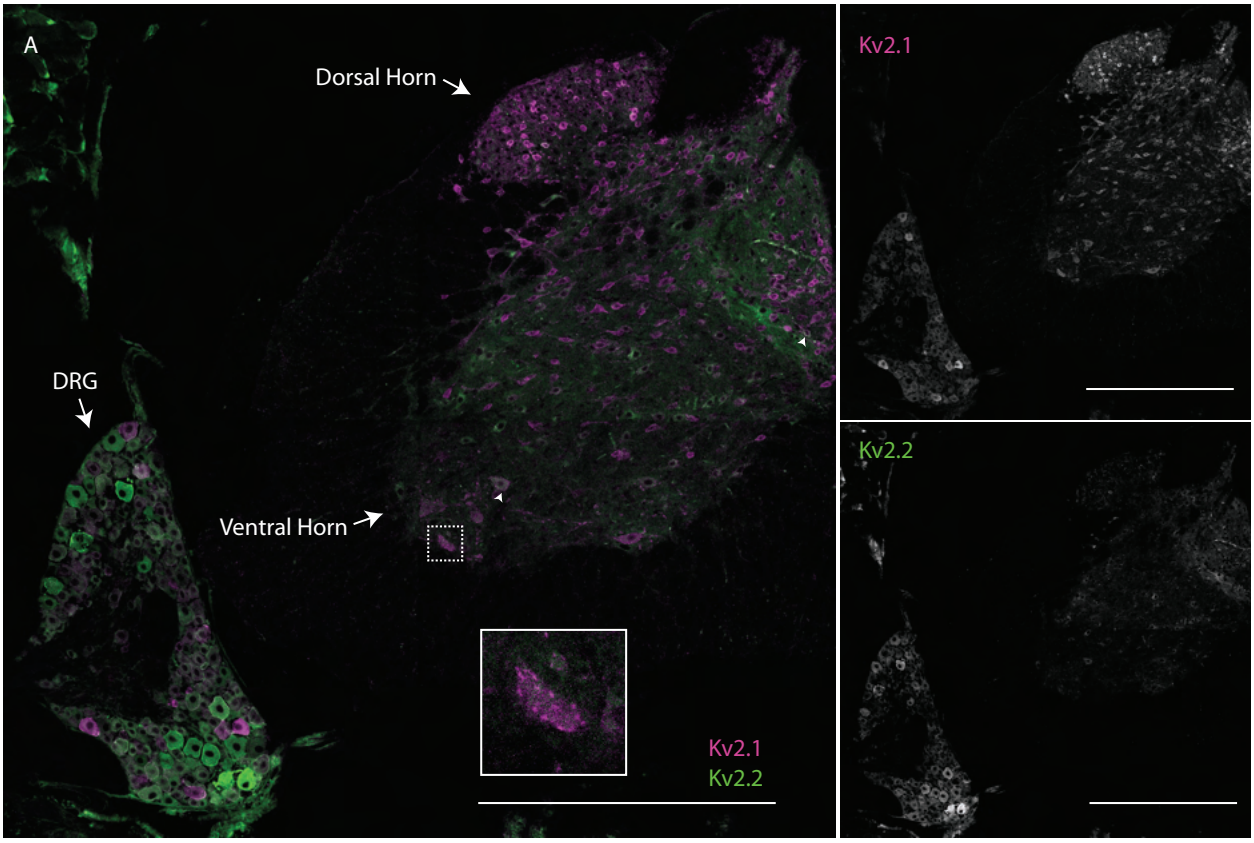

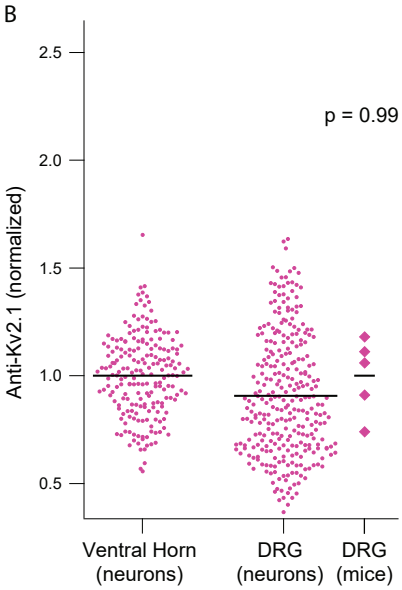

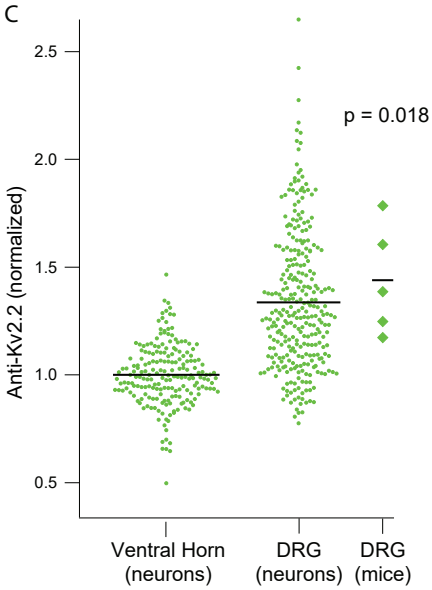

969

970

971 **Figure 6 legend**

972 DRG neurons have enriched Kv2.2 protein compared to neurons in the spinal cord. ***A***, Anti-
973 Kv2.1 (magenta) and anti-Kv2.2 (green) immunofluorescence in a spinal cord section from the
974 2nd lumbar vertebra (left). Anti-Kv2.1 immunofluorescence (right top) and anti-Kv2.2
975 immunofluorescence (right bottom). Arrows show neurons in the spinal cord with punctate
976 anti-Kv2.1 immunofluorescence. Arrow heads show neurons in the spinal cord with anti-Kv2.2
977 immunofluorescence. Scale bars are 500 µm. ***B***, Anti-Kv2.1 immunofluorescence from individual
978 neuron profiles (circles) from multiple mice in the DRG and ventral horn normalized to the
979 average fluorescence intensity of neuron profiles in the ventral horn. Diamonds to the right of
980 data represent the average intensity of individual mice. Significant differences from 1 were
981 calculated for individual mice using Students t-test. N = 5 mice, n = 295 in DRG and n = 200 in
982 ventral horn. Detailed information on each mouse used can be found in table 1. ***C***, Identical
983 analysis as in panel B but with anti-Kv2.2 immunofluorescence.

984

Figure 7

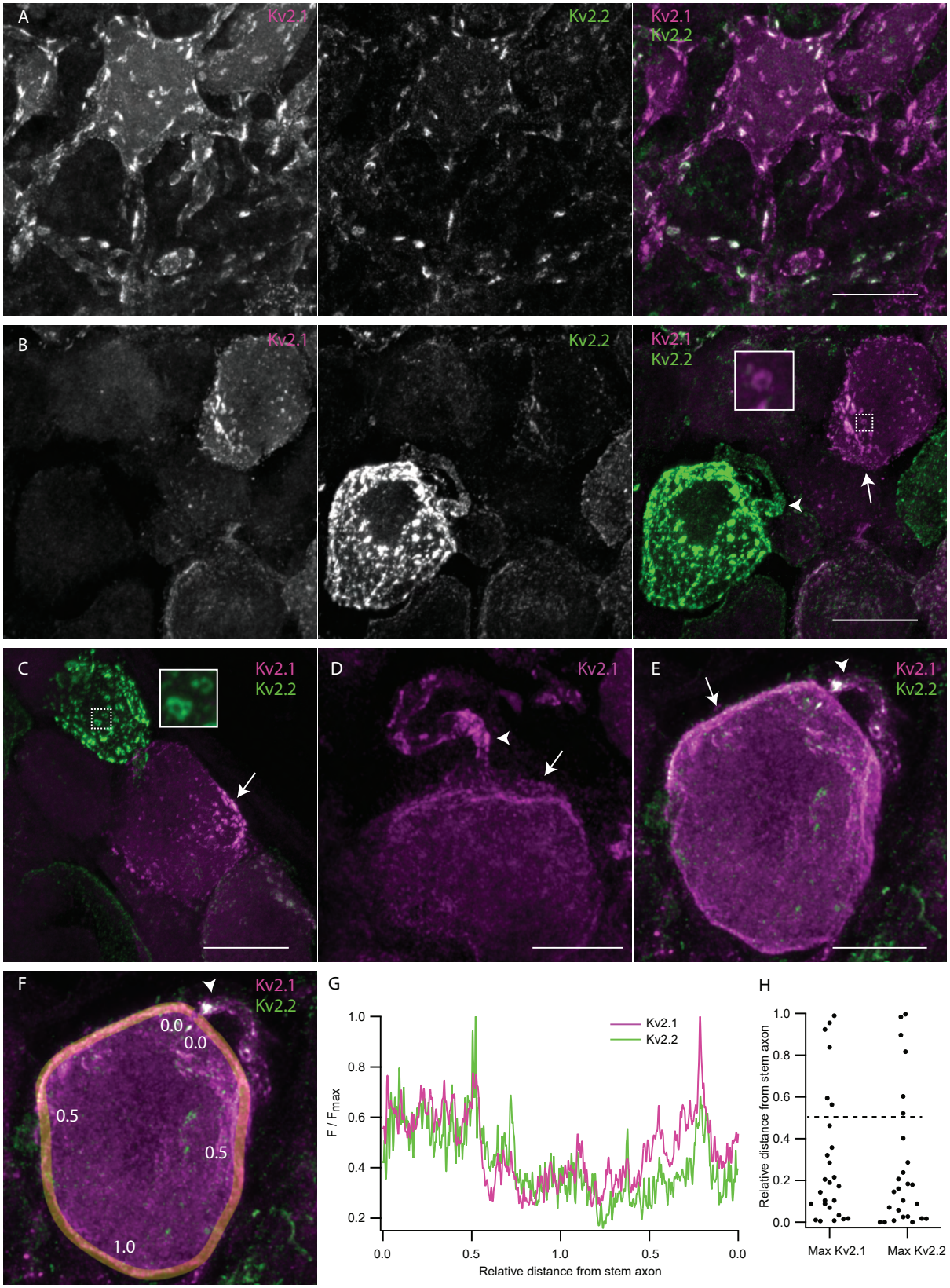
A
Kv2.1
Kv2.2
Kv2.1
Kv2.2
B
Kv2.1
Kv2.2
Kv2.1
Kv2.2
C
Kv2.1
Kv2.2
D
Kv2.1
E
Kv2.1
Kv2.2
F
Kv2.1
Kv2.2
0.0
0.0
0.5
0.5
1.0
G
Kv2.1
Kv2.2
F / Fmax
1.0
0.8
0.6
0.4
0.2
0.0
0.5
1.0
0.5
0.0
Relative distance from stem axon
H
Relative distance from stem axon
1.0
0.8
0.6
0.4
0.2
0.0
Max Kv2.1
Max Kv2.2

987 **Figure 7 legend**

988 Kv2 channels form clusters on DRG neuron somas and stem axons that are distinct from Kv2
989 channel clusters on ventral horn neurons. ***A***, Z-projection of anti-Kv2.1 and anti-Kv2.2
990 immunofluorescence in a ventral horn neuron from the 1st lumbar vertebra of a 7 week old
991 male mouse. ***B***, Z-projection of anti-Kv2.1 and anti-Kv2.2 immunofluorescence in DRG neurons
992 from the same mouse and section of the spinal column as neuron shown in A. Inset is
993 enlargement of the Kv2.1 donut cluster in dotted box. ***C***, Z-projection of anti-Kv2.1 and anti-
994 Kv2.2 immunofluorescence in DRG neurons from the same mouse as A and B. Inset is
995 enlargement of the Kv2.2 donut cluster in dotted box. ***D***, Z-projection of anti-Kv2.1
996 immunofluorescence in DRG neuron from the 13th thoracic DRG of a 24 week old male mouse.
997 ***E***, Z-projection of anti-Kv2.1 and anti-Kv2.2 immunofluorescence in DRG neuron from same
998 mouse in D. ***F***, Exemplar ROI for analyzing localization of Kv2 channel density relative to stem
999 axon. Same image as E. ROI line width is 1.24 µm. Numbers along line indicate approximate
1000 distance from stem axon normalized to the midpoint of the line. ***G***, Anti-Kv2.1 (magenta) and
1001 anti-Kv2.2 (green) immunofluorescence intensity along the ROI shown in F. Distance along the
1002 line was normalized such that the stem axon is 0 and the midpoint of the line is 1. ***H***, Analysis of
1003 the relative distance from the stem axon of the max anti-Kv2.1 or anti-Kv2.2
1004 immunofluorescence. Dotted line represents the middle of neurons relative to the stem axon.
1005 In all images arrows indicate asymmetrical clusters of Kv2 channels while arrow heads indicate
1006 the apparent stem axons. Display settings are not identical between images. Scale bars are 20
1007 µm.

1008

1009 **Figure 8**

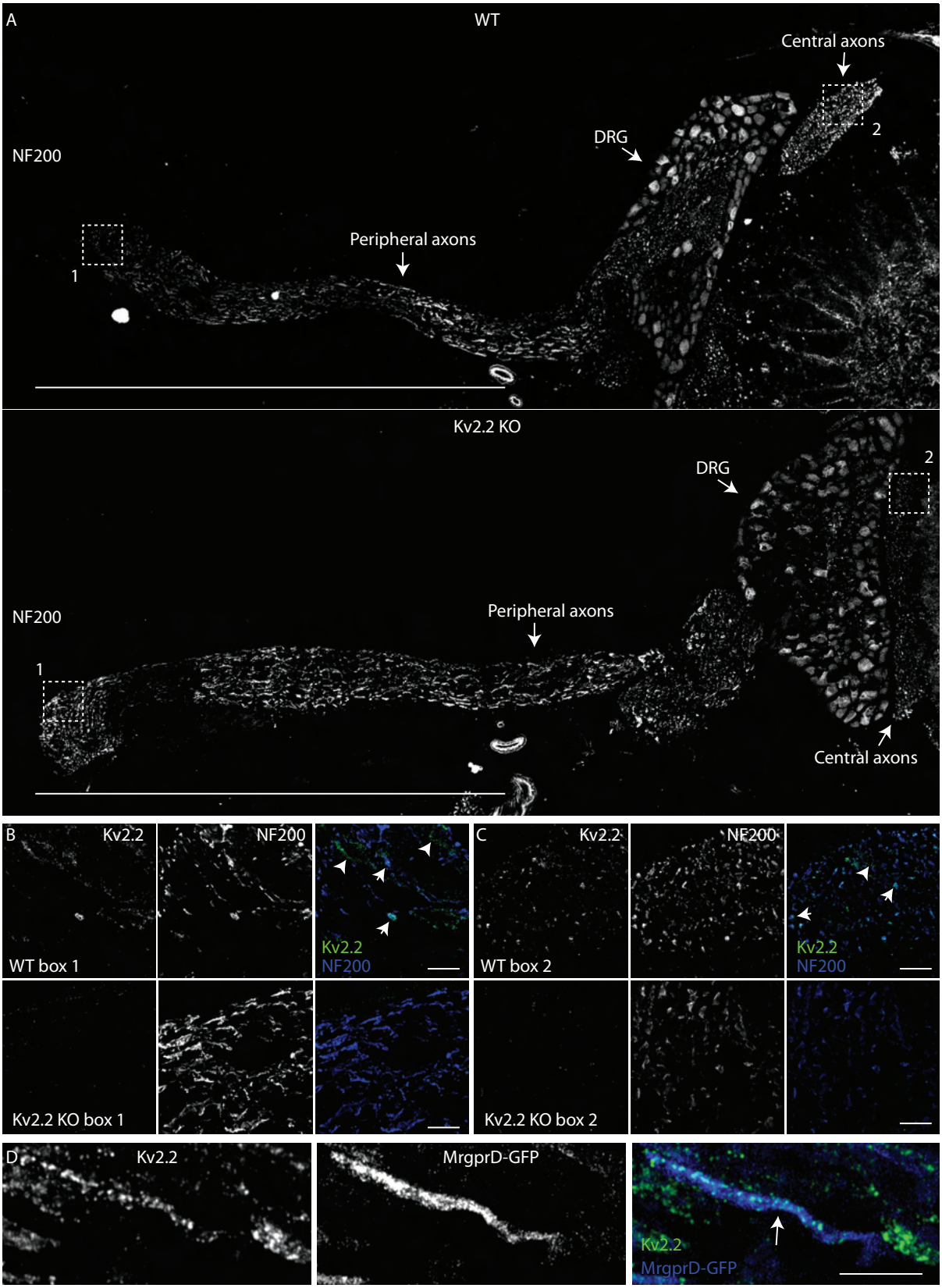

1010

1011 **Figure 8 legend**

1012 Kv2.2 channels are expressed in peripheral axons of DRG neurons. ***A***, WT (top) and Kv2.2 KO

1013 (bottom) sections containing the DRG, peripheral and central axons from the 1st lumbar DRG in

1014 age and sex matched 7 week old mice immunolabeled for NF200 (white). Scale bar is 1 mm. ***B***,

1015 High magnification z-projection of anti-Kv2.2 and anti-NF200 immunofluorescence from box 1

1016 in A of WT and Kv2.2 KO mice. Arrows indicate myelinated axons which show prominent anti-

1017 Kv2.2 immunofluorescence. Scale bars are 20 µm. ***C***, High magnification z-projection of anti-

1018 Kv2.2 and anti-NF200 immunofluorescence from box 2 in A of WT and Kv2.2 KO mice. Arrows

1019 indicate myelinated axons which show prominent anti-Kv2.2 immunofluorescence. Scale bars

1020 are 20 µm. ***D***, High magnification z-projection of anti-Kv2.2 immunofluorescence and MrgprD-

1021 GFP fluorescence in the peripheral axons of the 12th thoracic DRG of a 13 week old MrgprD-GFP

1022 mouse. Arrow indicates anti-Kv2.2 immunofluorescence on a GFP^{+} axon. Scale bar is 10 µm.

1023

1024 **Figure 9**

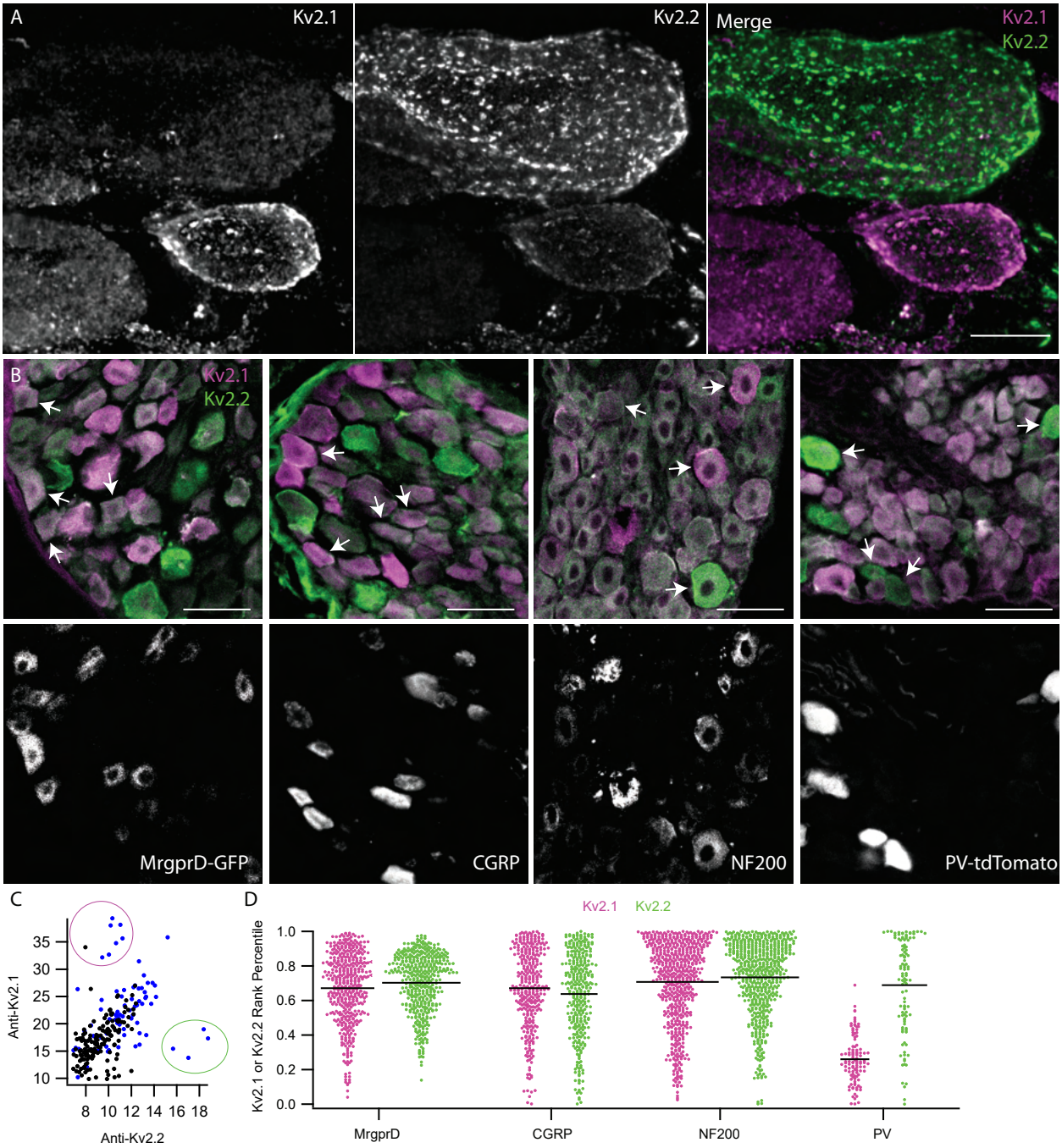

1025

1026 **Figure 9 legend**

1027 Anti-Kv2 immunofluorescence intensities are non-uniform across DRG neuron subtypes. ***A***,

1028 Exemplar z-projection of enrichment of anti-Kv2.1 (magenta) or anti-Kv2.2 (green)

1029 immunofluorescence in neighboring neurons. DRG section is from a 10 week old male mouse.
1030 Scale bar is 10 µm. ***B***, Top images show anti-Kv2.1 (magenta) and anti-Kv2.2 (green)
1031 immunofluorescence in DRG sections where subpopulation specific markers were used to
1032 identify, from left to right, non-peptidergic nociceptors, peptidergic nociceptors, myelinated
1033 neurons and proprioceptors. Fluorescence from specific markers is shown in bottom panels.
1034 Arrows indicate four exemplar neurons that have clear positivity for each subpopulation
1035 identified by fluorescence in lower panels. CGRP and NF200 subpopulations were identified
1036 using anti-CGRP and anti-NF200 antibodies while MrgprD-GFP and PV-tdTomato
1037 subpopulations were from transgenic mouse lines. Scale bars are 50 µm. ***C***, Scatter plot of anti-
1038 Kv2.1 and anti-Kv2.2 immunofluorescence of individual neuron profiles. Each point represents
1039 one profile. Magenta circle highlights the subpopulation of profiles that have high anti-Kv2.1
1040 but low anti-Kv2.2 immunofluorescence while the green circle highlights the subpopulation of
1041 profiles that have high anti-Kv2.2 but low anti-Kv2.1 immunofluorescence. Blue points
1042 represent myelinated DRG neuron profiles identified by NF200 immunofluorescence. ***D***, Ranked
1043 anti-Kv2.1 immunofluorescence (magenta points) or ranked anti-Kv2.2 immunofluorescence
1044 (green points) of individual profiles from subpopulations shown in B. Only profiles that were
1045 positive for each marker are shown. Each point represents one profile. MrgprD population N = 4
1046 mice, CGRP population N = 3 mice, NF200 population N = 3 mice and PV population N = 2 mice.
1047 Detailed information on each mouse used can be found in table 1.
1048

1049 **Figure 10**

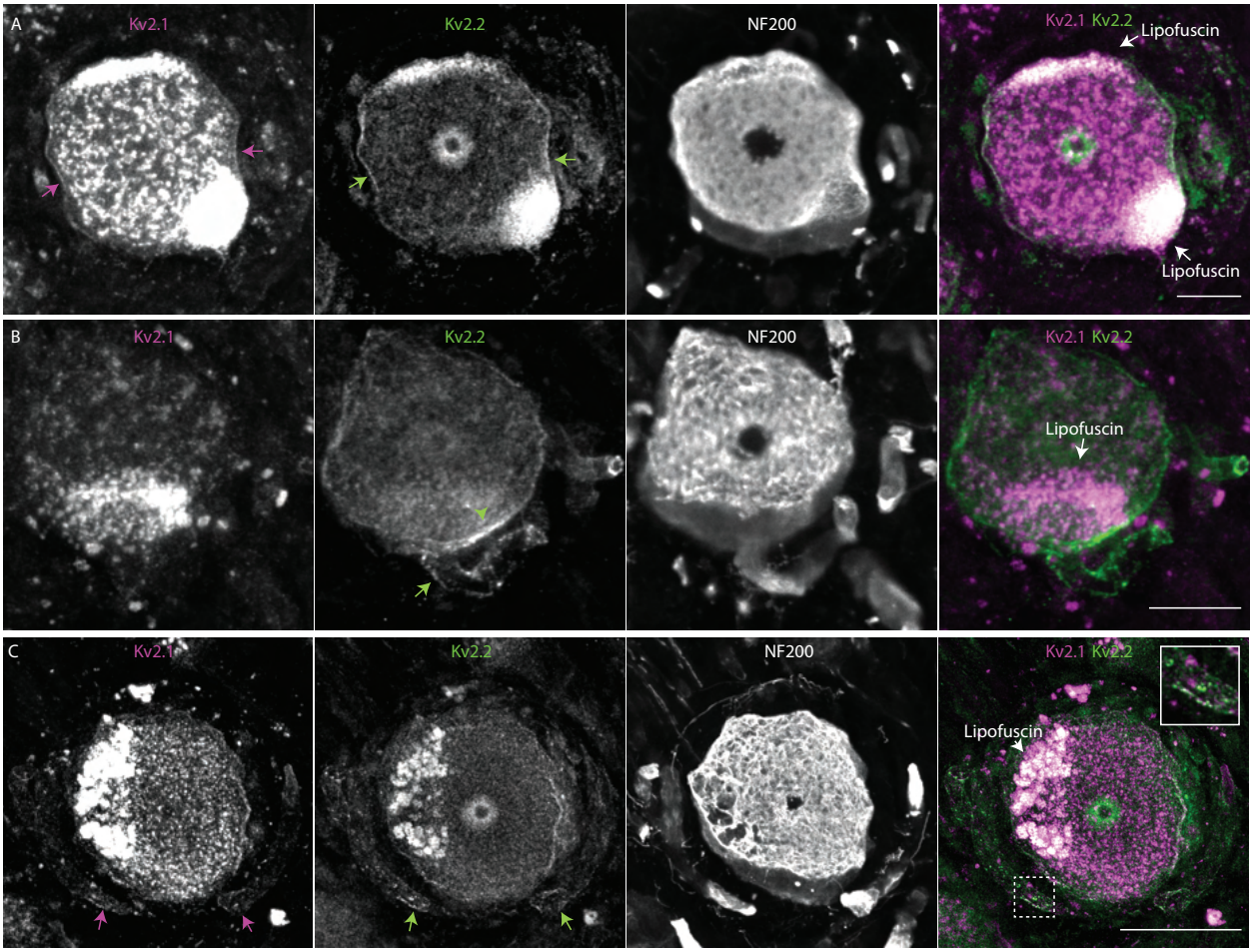

1050

1051 **Figure 10 legend**

1052 Kv2 channel expression and localization in human DRG neurons is similar to mice. ***A***,

1053 Immunofluorescence from human DRG neurons labeled with anti-Kv2.1 and anti-Kv2.2

1054 antibodies. Autofluorescence attributed to lipofuscin is labeled in right panel while apparent

1055 Kv2.1 and Kv2.2 protein are labeled in left and middle panel respectively. Scale bar is 50 µm. ***B***,

1056 Z-projection of anti-Kv2.2 (left) and anti-NF200 immunofluorescence (middle) of human DRG

1057 neuron somata. Green arrow head indicates asymmetric distribution of Kv2.2 clusters on

1058 neuron soma, green arrow indicates the apparent stem axon. Scale bar is 20 µm. ***C***, Z-projection

1059 of anti-Kv2.1 (upper left), anti-Kv2.2 (upper right) and anti-NF200 (lower left)

1060 immunofluorescence of a human DRG neuron. Magenta and green arrows indicate Kv2.1 and
1061 Kv2.2 respectively on the apparent stem axon. Inset shows expansion of dotted line boxes
1062 which highlights Kv2.1 and Kv2.2 clusters on the apparent stem axon. Autofluorescence
1063 attributed to lipofuscin is labeled in lower right panel. Scale bar is 50 µm. All images are from
1064 donor #1. Detailed information on each donor can be found in the *Human Tissue Collection*
1065 section of the methods.
1066

1067 **SUPPLEMENTAL FIGURES**

1068 **Supplemental Figure 1**

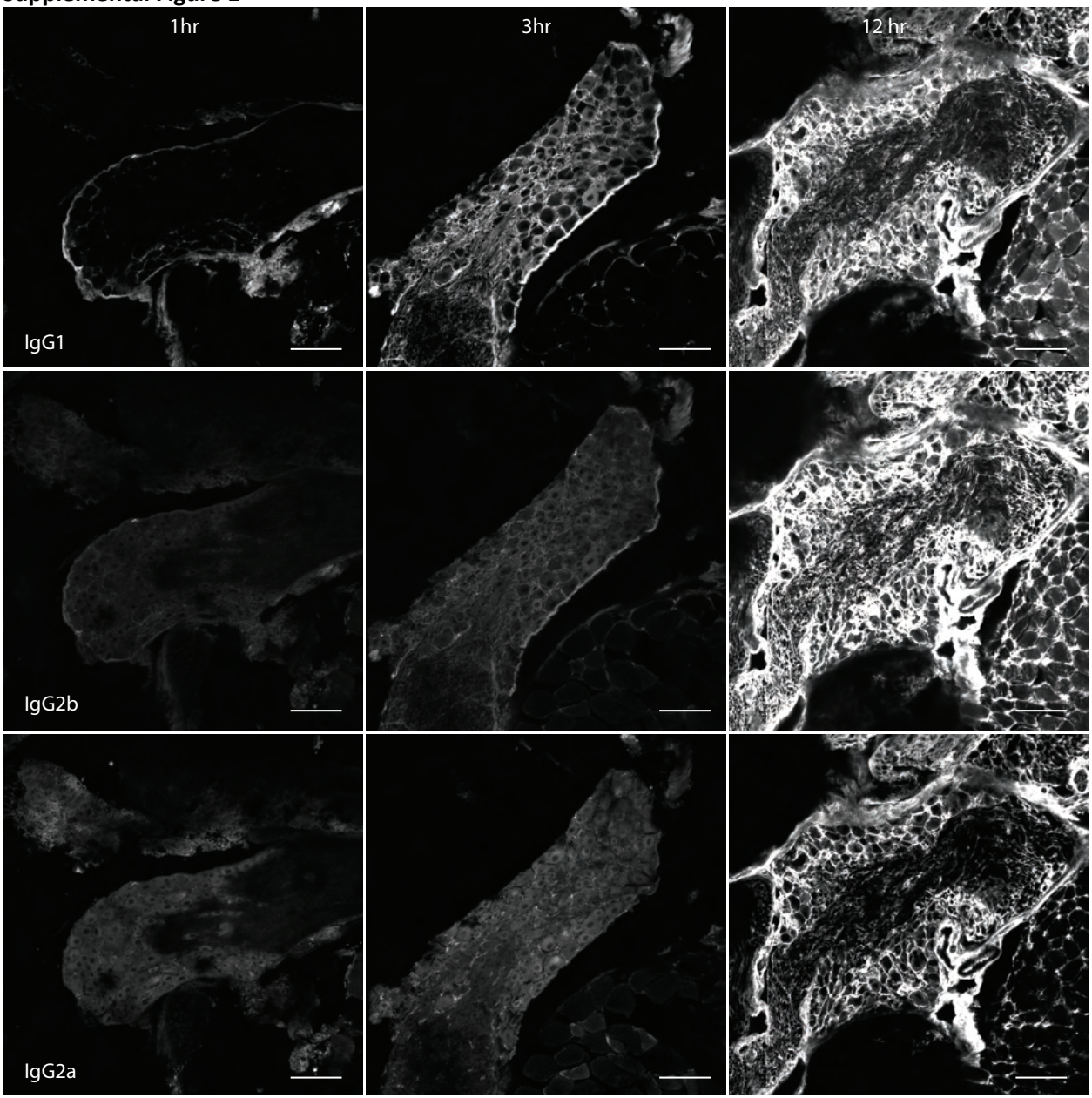

1069

1070 **Supplemental Figure 1 legend**

1071 Off-target mouse anti-IgG1, IgG2b, and IgG2a immunofluorescence increases with fixation time.
1072 Images of DRG sections labeled with fluorescently tagged antibodies which target IgG1 (top),
1073 IgG2b (middle) and IgG2a (bottom) after DRG were fixed in ice cold 4% PFA for 1, 3 and 12
1074 hours. DRG sections are from the same mouse. Scale bars are 100 µm.

1075

1076 **Supplemental Figure 2**

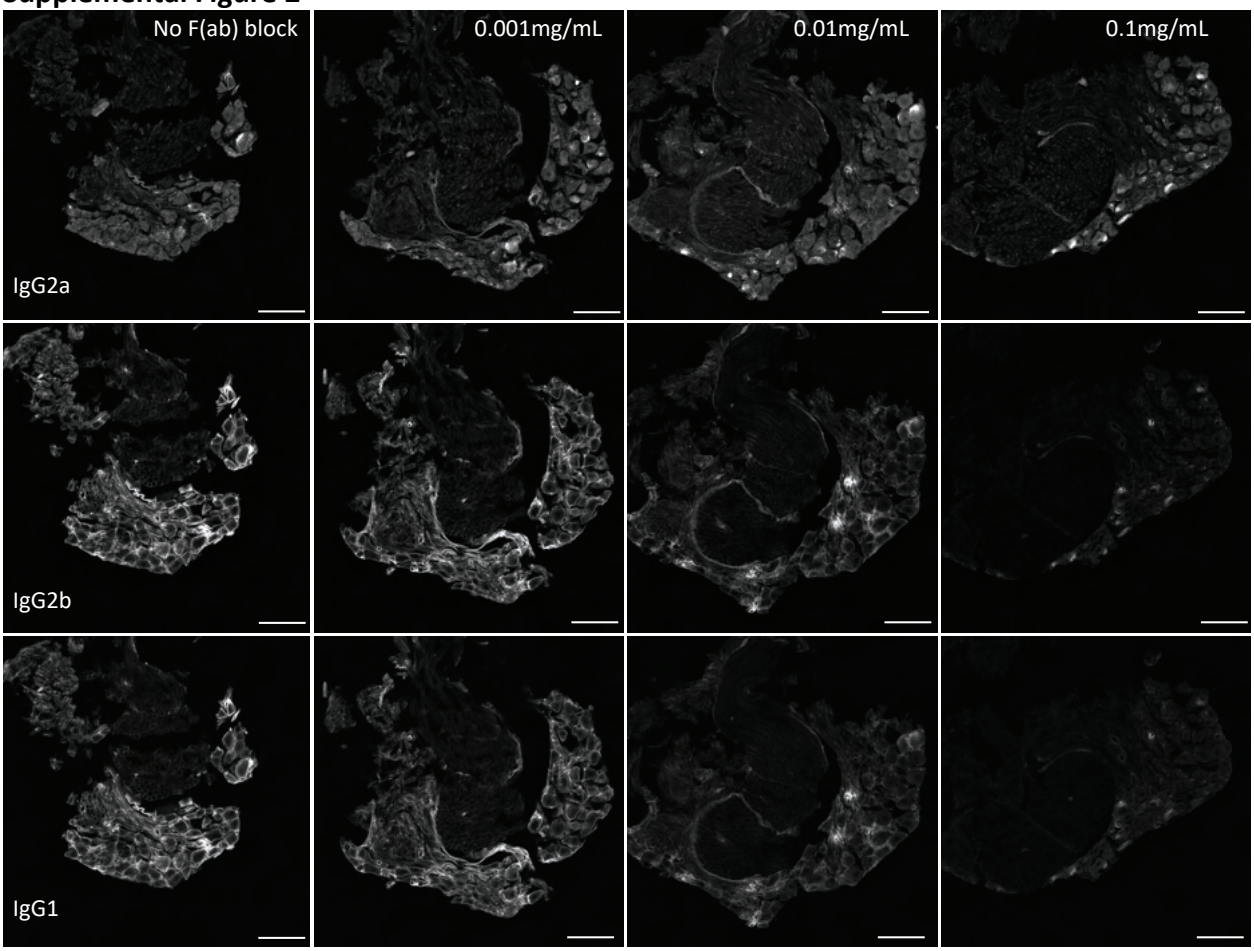

1077

1078 **Supplemental Figure 2 legend**

1079 Pre-incubation of mouse DRG sections in IgG H+L Fab fragments reduces off target secondary
1080 antibody labeling. Representative images of DRG sections from the same DRG treated with
1081 increasing concentrations (left to right) of IgG H+L Fab fragment and the same concentration of
1082 secondary antibody used in experiments throughout this study. Images were taken with
1083 identical imaging settings and are set to the same brightness and contrast. Scale bars are 100
1084 µm.

1085 **Supplemental Figure 3**

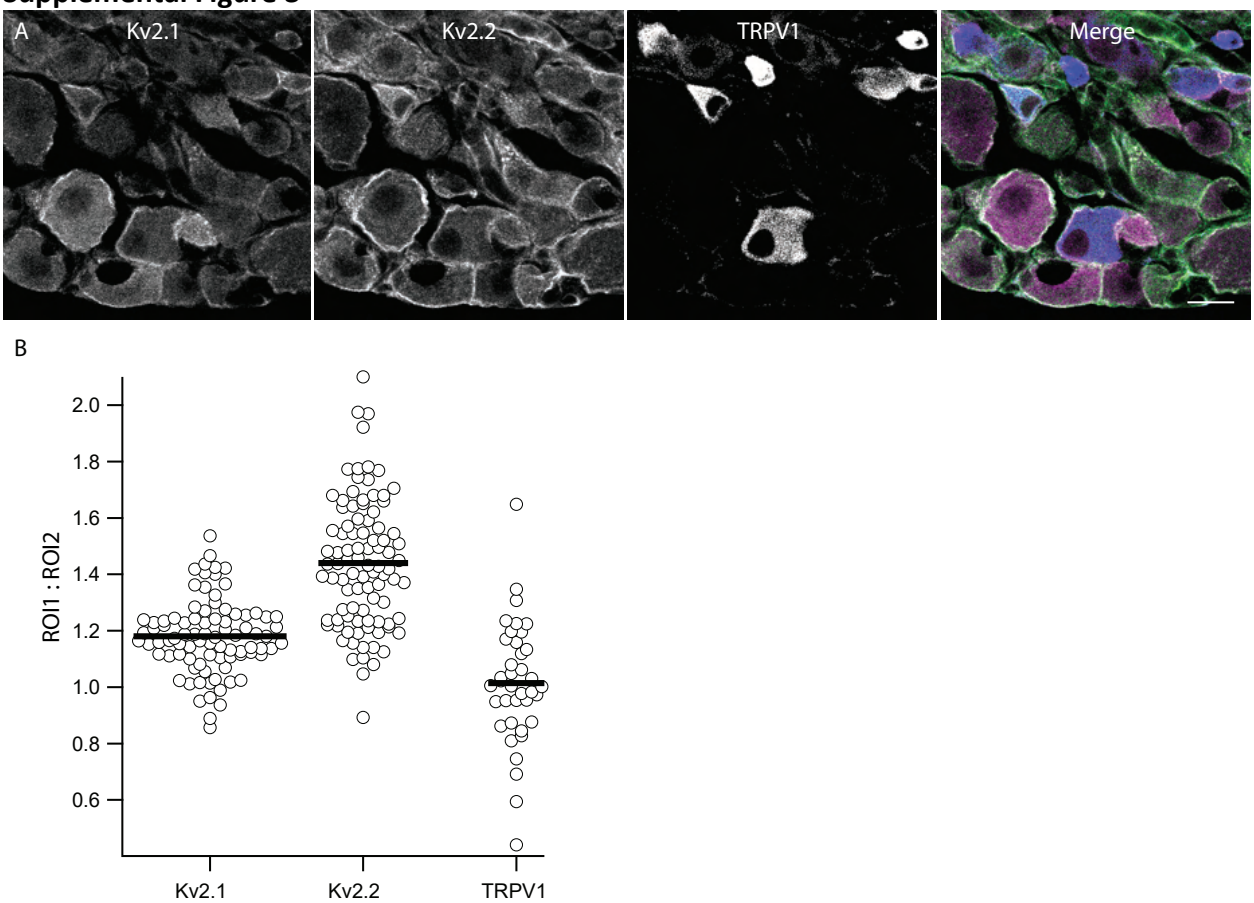

1086
1087 **Supplemental Figure 3 legend**
1088 Kv2.1 and Kv2.2 protein are enriched at the outer edge of DRG neuron somas relative to TRPV1.
1089 ***A***, Anti-Kv2.1, anti-Kv2.2 and anti-TRPV1 immunofluorescence from lumbar DRG neurons.
1090 Prominent cytoplasmic anti-TRPV1 immunofluorescence was observed in a subset of small
1091 diameter neurons. In merge image anti-Kv2.1, anti-Kv2.2 and anti-TRPV1 immunofluorescence
1092 are magenta, green and blue respectively. Scale bar is 20 µm. ***B***, Ratio of average anti-Kv2.1,
1093 anti-Kv2.2 or anti-TRPV1 immunofluorescence from outer and inner ROIs for individual
1094 neurons.
1095
1096

1097 **Supplemental Figure 4**

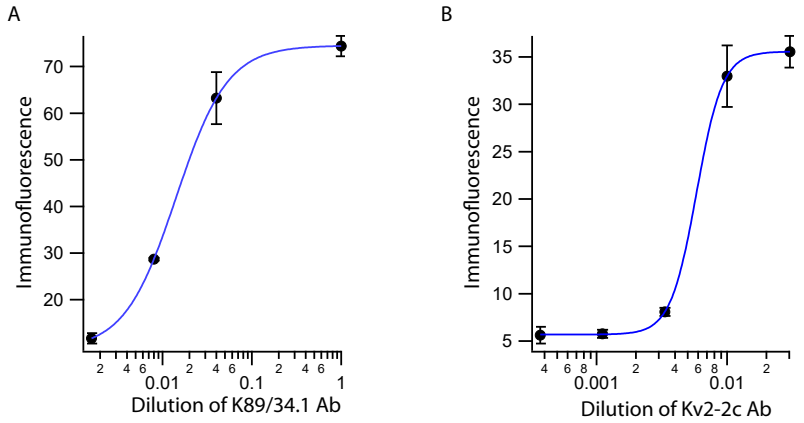

1098

1099 **Supplemental Figure 4 legend**

1100 Kv2 antibodies used in knockout experiments are at saturating concentrations. ***A***,
1101 Concentration response of immunofluorescence from sections labeled with anti-Kv2.1 antibody
1102 used in Figure 2. Blue line is a Hill fit of the data. 1:1 = 2 sections, 1:25 = 3 sections, 1:125 = 2
1103 sections, 1:625 = 3 sections ***B***, Concentration response of immunofluorescence from sections
1104 labeled with anti-Kv2.2 antibody used in Figure 3. Blue line is a Hill fit of the data. 1:33 = 2
1105 sections, 1:100 = 10 sections, 1:300 = 4 sections, 1:900 = 4 sections, 1:2700 = 3 sections

1106

1107 **Supplemental Figure 5**

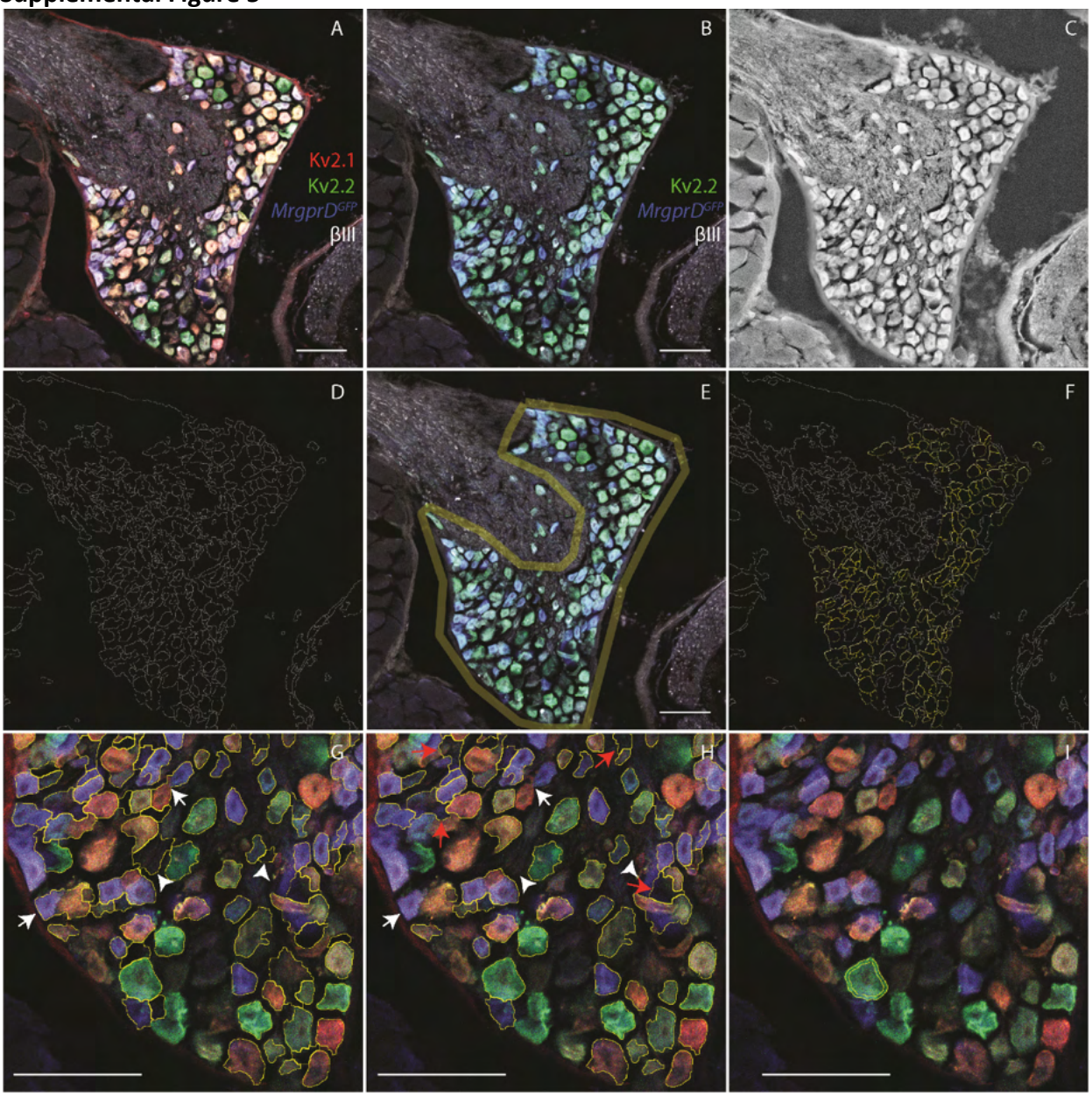

1108

1109 **Supplemental Figure 5 legend**

1110 A method to sample neurons in DRG imaging data using watershed segmentation identifies the
1111 outer region of neurons. ***A***, Image of anti-Kv2.1, anti-Kv2.2, anti-βIII tubulin
1112 immunofluorescence and MrgprD-GFP fluorescence. ***B***, Same image as A with anti-Kv2.1
1113 immunofluorescence channel removed as this is an example of processing data for Kv2.1 KO
1114 analysis. ***C***, Grayscale image of average fluorescence from all three channels shown in B.
1115 Gaussian and median filters were applied to image to improve watershed segmentation. ***D***,
1116 Watershed segmentation of image in C using the MorphoLibJ Morphological Segmentation
1117 Plugin in Fiji. ***E***, Example of manually drawn boundary that encompasses the neuron somas in
1118 the DRG so that only these watershed lines are selected. ***F***, Selected ROIs from watershed
1119 segmentation (yellow). ROIs were excluded based on roundness and size using the Analyze

1120 Particles tool in Fiji. ***G***, ROIs in F overlaid on DRG image showing that some ROIs are selecting
1121 regions that do not contain neurons (arrow heads) or are selecting multiple neurons (arrows).
1122 ***H***, ROIs after processing using an in-house R script which removes ROIs that do not contain
1123 neurons (arrow heads) and ROIs that contain two neurons (arrows). This script did not remove
1124 all ROIs that do not contain neurons (red arrows). Each experiment performed was done
1125 alongside controls where the primary antibodies were omitted and fluorescence from these
1126 control sections was used by the in-house R script to identify and remove ROIs that do not
1127 contain neurons. ***I***, Example of automatically generated annulus that encompasses the outer
1128 edge of the soma. Scale bars are 100 µm.
1129

1130 **Supplemental Figure 6**

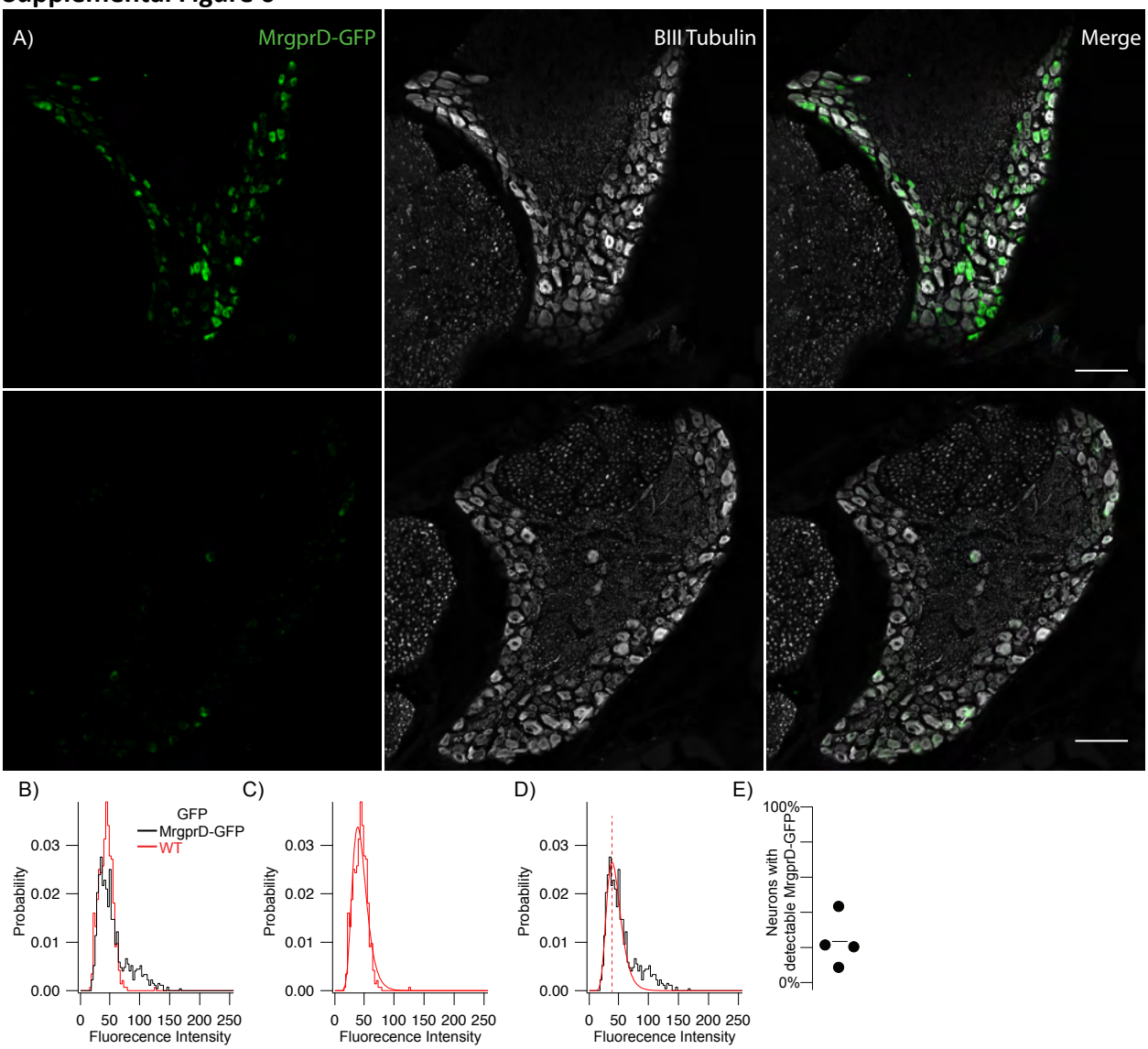

1131
1132 **Supplemental Figure 6 legend**

1133 Method used to estimate percent of neurons expressing Kv2.1 and Kv2.2 reliably predicts the
1134 percentage of neurons that express GFP in MrgprD-GFP mice. ***A***, MrgprD-GFP (top) and WT
1135 (bottom) DRG sections immunolabeled for BIII tubulin (white). Images were taken with identical
1136 imaging settings and are set to the same brightness and contrast. Scale bars are 100 µm. ***B***,
1137 Distribution of fluorescence intensity from MrgprD-GFP (black) and WT (red) neurons. Data
1138 represents the fluorescence intensity of 905 MrgprD-GFP neurons from 9 DRG sections from 1
1139 mouse or 477 WT neurons from 5 DRG sections from 1 mouse. DRG sections were taken from 7
1140 week old female mice and are from the 1st lumbar DRG. ***C***, WT data shown in B fit with a log
1141 normal distribution (red fit). ***D***, MrgprD-GFP data shown in B fit with the WT distribution (red
1142 fit) where width and mean were constrained to the WT distribution and amplitude was
1143 unconstrained (equation 1). Only MrpgrD-GFP data to the left of the mean intensity of WT
1144 neurons (red dotted line) was used for the fit. ***E***, Percent of neurons with detectable GFP
1145 protein of 4 mice (3 females 1 male). All DRG sections were taken from the 1st lumbar DRG.

1146 **Supplemental Figure 7**

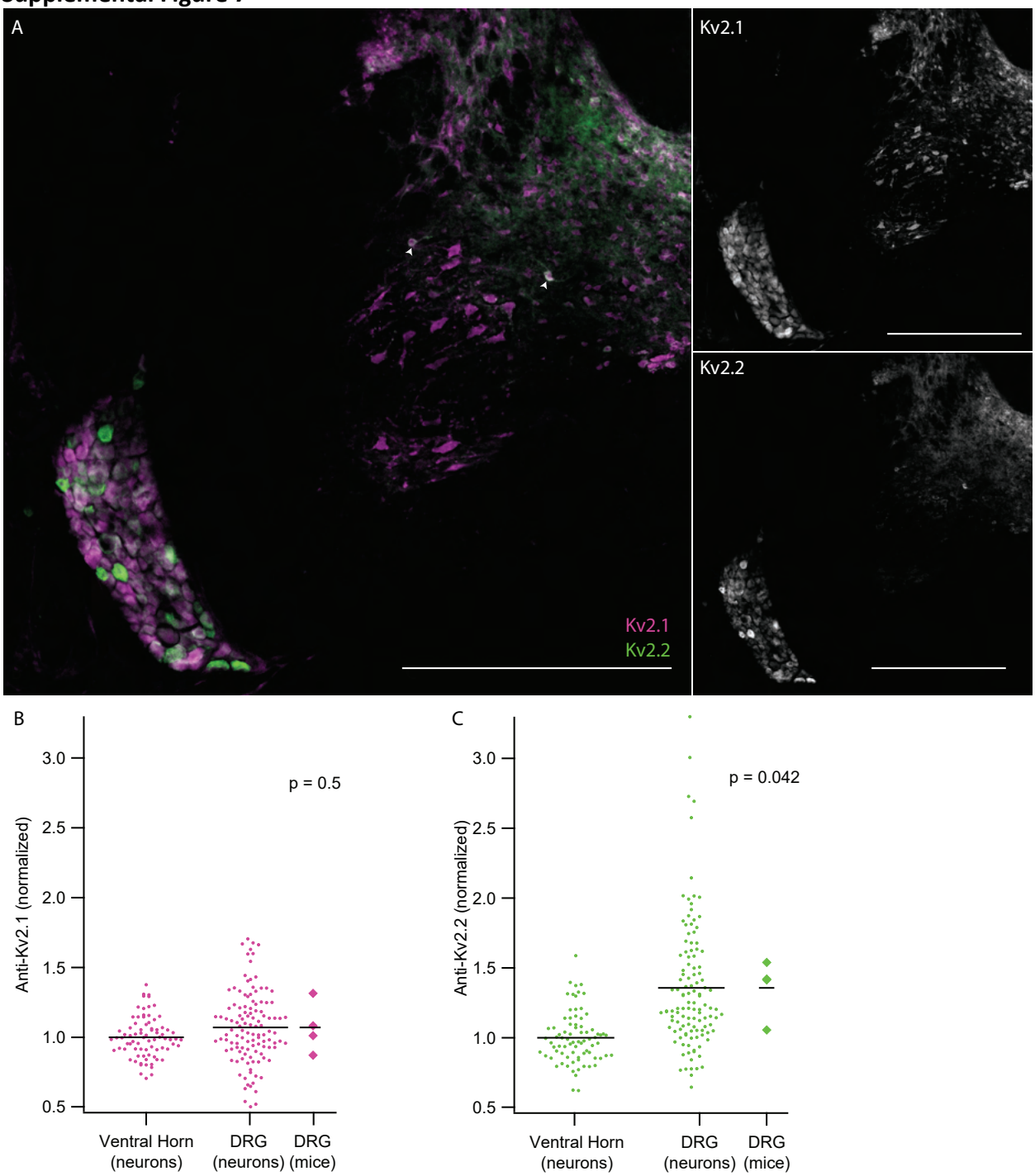

1147

1148 **Supplemental Figure 7 legend**

1149 DRG neurons have enriched Kv2.2 protein compared to neurons in the ventral horn. ***A***, Anti-
1150 Kv2.1 (magenta) and anti-Kv2.2 (green) immunofluorescence in a spinal cord section from the
1151 13th thoracic vertebra (left). Anti-Kv2.1 immunofluorescence (right top) and anti-Kv2.2
1152 immunofluorescence (right bottom). Arrow heads show neurons in the spinal cord with anti-
1153 Kv2.2 immunofluorescence. Scale bars are 500 µm. ***B***, Anti-Kv2.1 immunofluorescence from

individual neurons (circles) in the DRG and ventral horn normalized to the average fluorescence intensity of neurons in the ventral horn. Diamonds to the right of data represent the average intensity in the DRG of individual mice. Significant differences from 1 were calculated for individual mice using Students t-test. N = 4 mice n = 116 in DRG and n = 77 in ventral horn. ***C***, Identical analysis shown in B with anti-Kv2.2 immunofluorescence.

1160 **Supplemental Figure 8**

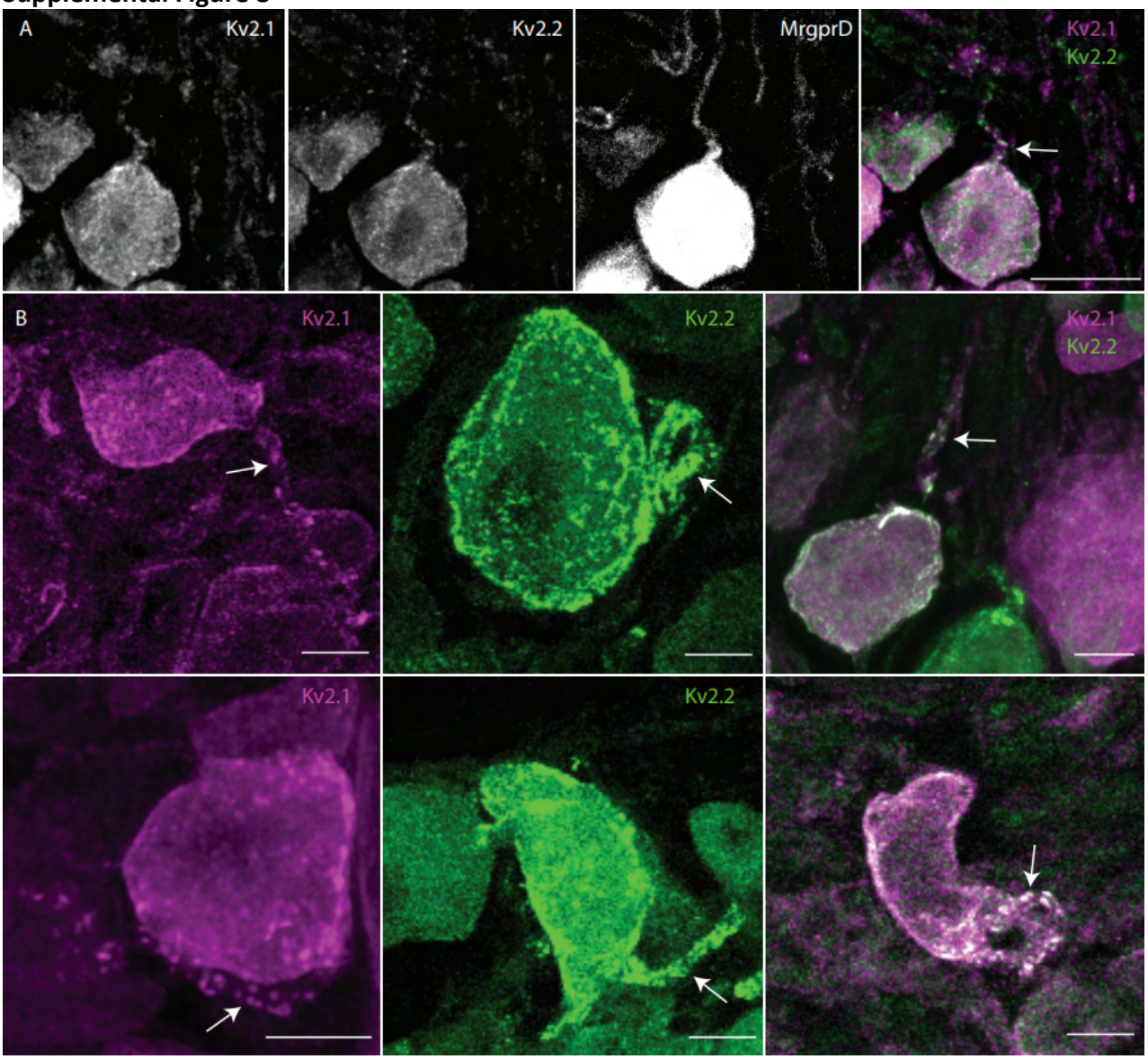

1161

1162 **Supplemental Figure 8 legend**

1163 Kv2 channels are expressed on the stem axon of mouse DRG neurons. ***A***, Z-projection with anti-
1164 Kv2.1 and anti-Kv2.2 immunofluorescence on the stem axon of a neuron in the DRG of a
1165 MrgprD-GFP mouse. ***B***, Gallery of z-projected images of DRG neurons with anti-Kv2.1 and/or
1166 anti-Kv2.2 immunofluorescence on stem axons. Arrows indicate stem axons. Scale bars are 10
1167 µm

Supplemental Figure 9

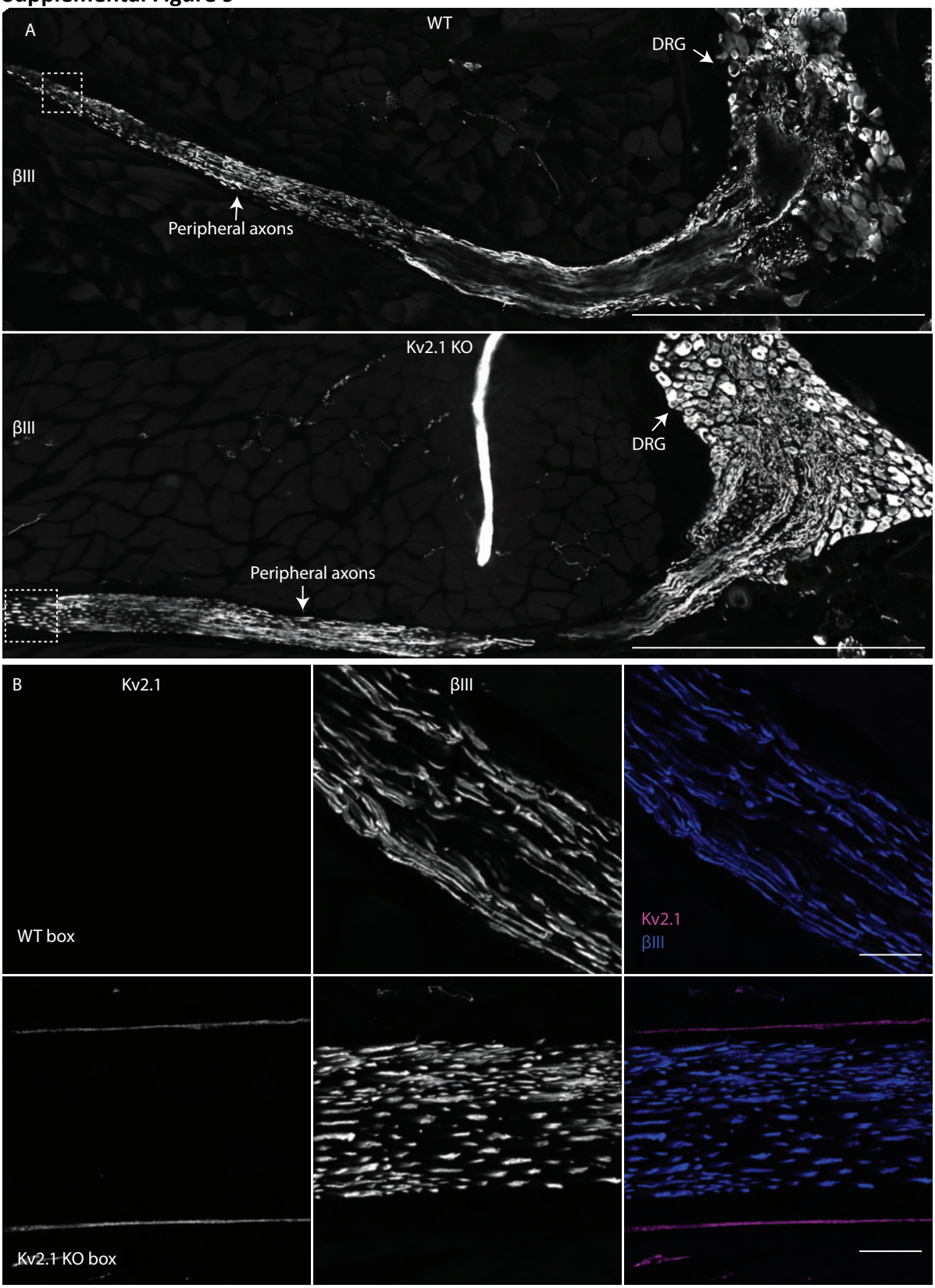

1170 **Supplemental Figure 9 legend**
1171 Kv2.1 channels were not detected in peripheral axons of DRG neurons. ***A***, WT (top) and Kv2.1
1172 KO (bottom) sections containing the DRG and peripheral axons from the 12th thoracic DRG in
1173 age and sex matched 7 week old mice immunolabeled for βIII tubulin (white). Scale bar is 500
1174 µm. ***B***, High magnification z-projection of anti-Kv2.1 and anti-βIII immunofluorescence from box
1175 in A of WT and Kv2.1 KO mice. Scale bars are 20 µm.
1176
1177

1178 **Supplemental Figure 10**

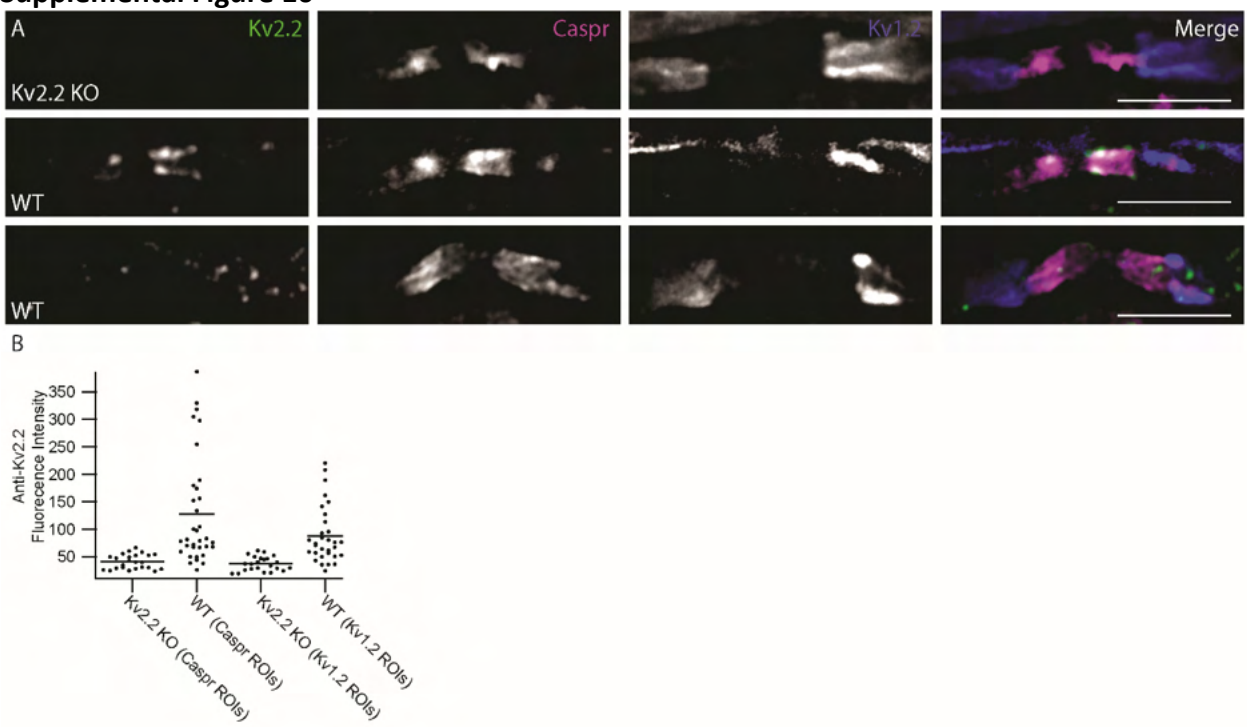

1179

1180 **Supplemental Figure 10 legend**

1181 Kv2.2 is expressed in myelinated fibers of DRG neuron axons. ***A***, Kv2.2 KO (top) and WT (middle
1182 and bottom) sections containing the peripheral axons from the 12th thoracic DRG in 28 week
1183 old mice immunolabeled for Kv2.2, Caspr and Kv1.2. Middle panels are an exemplar of
1184 prominent Kv2.2 immunofluorescence in CASPR labeled axons and bottom panels are an
1185 exemplar of prominent Kv2.2 clusters in the Kv1.2 labeled axons. Scale bars are 5 µm. ***B***,
1186 Analysis of anti-Kv2.2 immunofluorescence intensity in CASPR and Kv1.2 labeled regions of age
1187 and sex matched WT and Kv2.2 KO mice. Individual points represent single ROIs drawn around
1188 anti-CASPR or anti-Kv1.2 immunofluorescence.

1189

1190

1191 **Supplemental Figure 11**

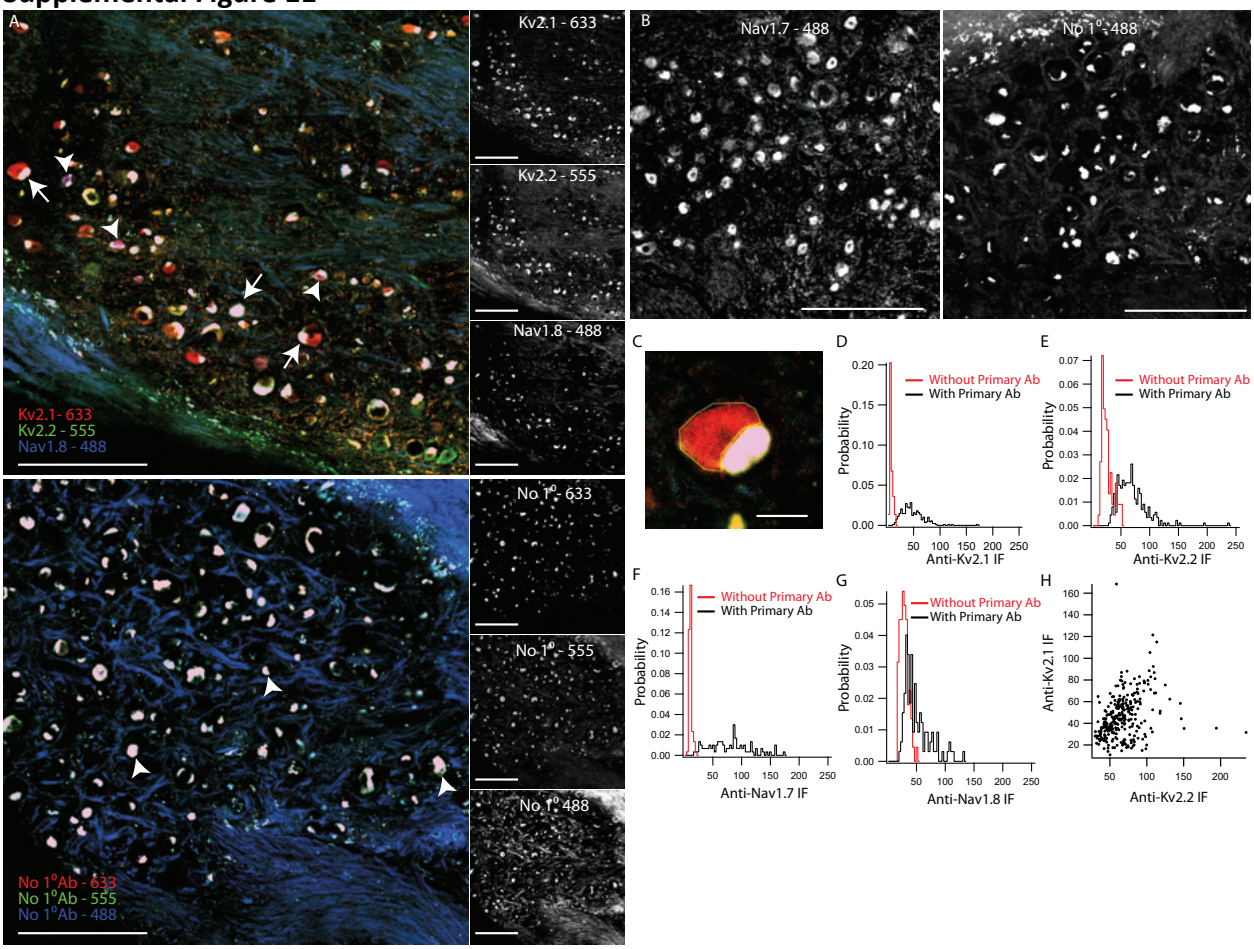

1192

1193 **Supplemental Figure 11 legend**

1194 Fluorescence from human DRG neurons labeled with ion channel targeting antibodies is distinct
1195 from human DRG neurons where ion channel targeting antibodies were omitted. ***A***, Top:
1196 Immunofluorescence from human DRG section labeled with anti-Kv2.1, anti-Kv2.2 and anti-
1197 Nav1.8 antibodies. Bottom: Fluorescence from human DRG section where the primary
1198 antibodies are omitted. Arrows in top and bottom images indicate examples of
1199 autofluorescence from apparent intracellular lipofuscin. Arrow heads in top image identify anti-
1200 Nav1.8 immunofluorescence. Images on the right are fluorescence from each fluorescence
1201 channel of the top and bottom images. Number next to target protein label represents
1202 excitation wavelength. DRG sections from top and bottom images are from the same DRG.
1203 Scale bars are 500 µm. ***B***, Left: Immunofluorescence from human DRG section labeled with anti-
1204 Nav1.7 antibody. Right: Fluorescence from human DRG section where the primary antibody has
1205 been omitted. Number next to target protein label represents excitation wavelength. DRG
1206 sections in left and right images are from the same DRG. Scale bars are 500 µm. ***C***, Exemplar
1207 manually drawn ROI to analyze fluorescence intensity in human DRG neurons that omits
1208 apparent lipofuscin autofluorescence. Scale bar is 50 µm. ***D***, Distribution of fluorescence
1209 intensity of human DRG neurons labeled with an anti-Kv2.1 antibody (black) or when the anti-
1210 Kv2.1 antibody was omitted (red). Data represents the fluorescence intensity of 293 neurons
1211 labeled with anti-Kv2.1 antibody or 73 neurons where the anti-Kv2.1 antibody was omitted. ***E***,

1212 Distribution of fluorescence intensity of human DRG neurons labeled with anti-Kv2.2 antibody
1213 (black) or when the anti-Kv2.2 antibody was omitted (red). Data represents the fluorescence
1214 intensity of 293 neurons labeled with anti-Kv2.2 antibody or 73 neurons where the anti-Kv2.2
1215 antibody was omitted. ***F***, Distribution of fluorescence intensity of human DRG neurons labeled
1216 with anti-Nav1.7 antibody (black) or when the anti-Nav1.7 antibody was omitted (red). Data
1217 represents the fluorescence intensity of 99 neurons labeled with anti-Nav1.7 antibody or 99
1218 neurons where the anti-Nav1.7 antibody was omitted. ***G***, Distribution of fluorescence intensity
1219 of human DRG neurons labeled with anti-Nav1.8 antibody (black) or when the anti-Nav1.8
1220 antibody was omitted (red). Data represents the fluorescence intensity of 293 neurons labeled
1221 with anti-Nav1.8 antibody or 73 neurons where the anti-Nav1.8 antibody was omitted. ***H***,
1222 Fluorescence intensity of human neurons labeled with both anti-Kv2.1 and anti-Kv2.2
1223 antibodies. Individual points represent individual neurons. All images are from donor #2.
1224 Detailed information on each donor can be found in the *Human Tissue Collection* section of the
1225 methods.
1226

1227 **Supplemental Figure 12**

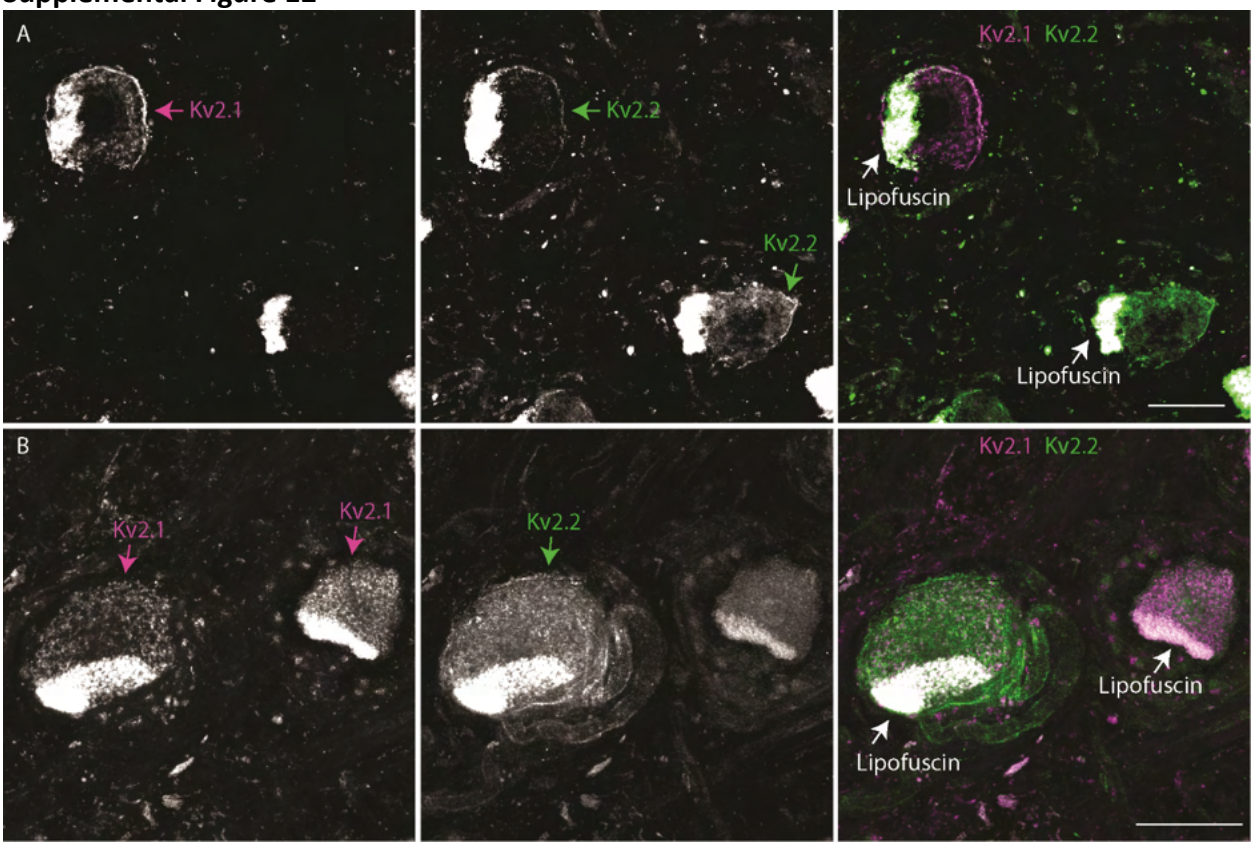

1228

1229 **Supplemental Figure 12 legend**

1230 Immunofluorescence from human DRG neurons from donor #2 ***A*** and donor #3 ***B*** labeled with
1231 anti-Kv2.1 and anti-Kv2.2 antibodies. Autofluorescence attributed to lipofuscin is labeled in
1232 right panels while apparent Kv2.1 and Kv2.2 protein are labeled in left and middle panels
1233 respectively. Scale bars are 50 µm. Detailed information on each donor can be found in the
1234 *Human Tissue Collection* section of the methods.

1235

1236 **Supplemental Figure 13**

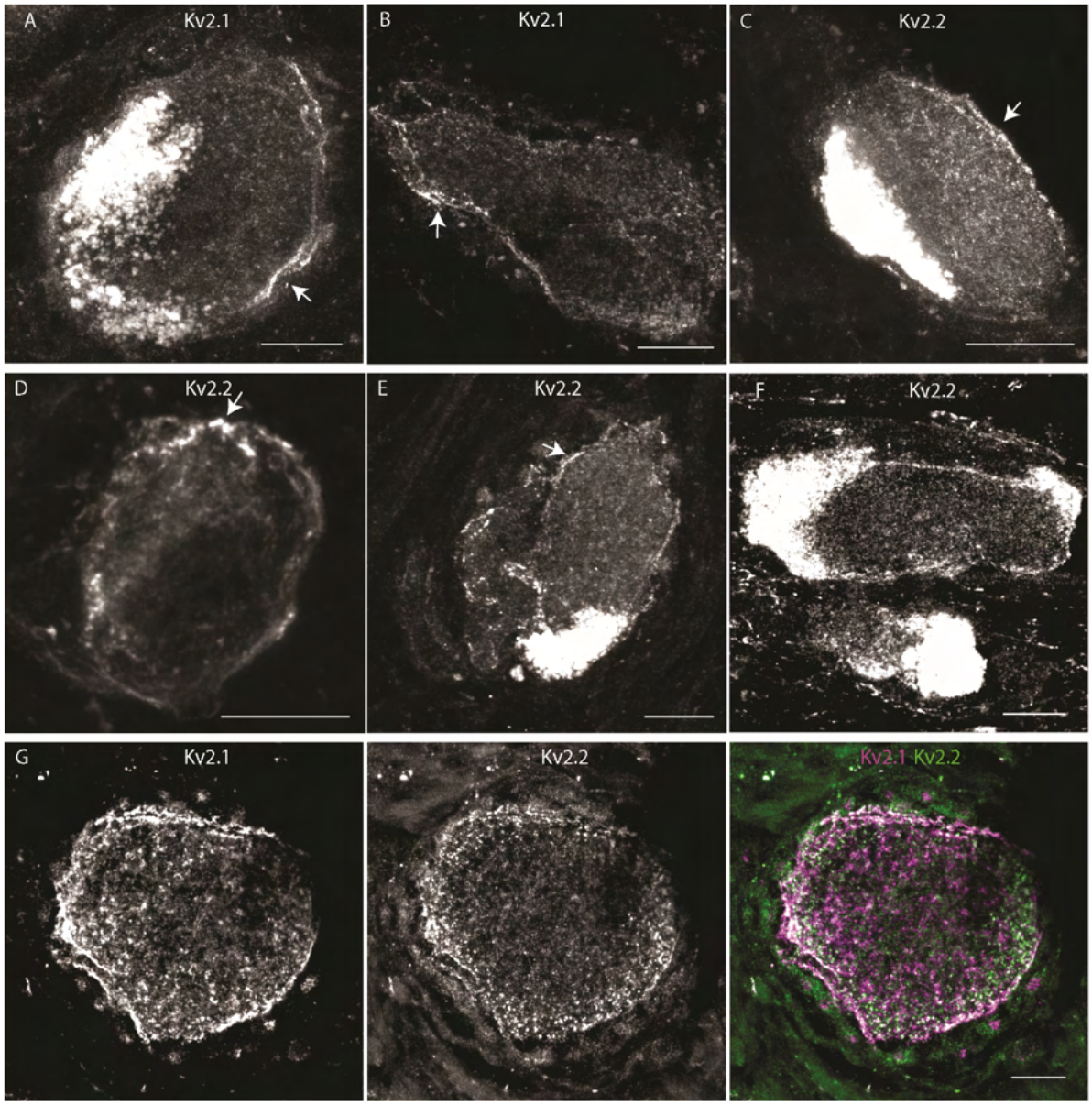

1237
1238 **Supplemental Figure 13 legend**
1239 Kv2 channels are enriched at the outer edge of human DRG neurons. ***A-B***, Exemplar z-
1240 projections of anti-Kv2.1 immunofluorescence enriched at the outer surface of human DRG
1241 neurons. Arrows indicate asymmetric clusters. Images are from donor #2 Scale bars are 20 µm.
1242 ***C-F***, Exemplar z-projections of anti-Kv2.2 immunofluorescence enriched at the outer surface of
1243 a human DRG neurons. Arrows indicate asymmetric clusters. Image in ***E*** is from donor #3 while
1244 all other images are from donor #2. Scale bars are 20 µm. ***G***, Exemplar z-projection of anti-Kv2.1
1245 and anti-Kv2.2 immunofluorescence both enriched at the outer surface of a human DRG neuron
1246 soma. Image is from donor #2. Scale bar is 20 µm. Detailed information on each donor can be
1247 found in the *Human Tissue Collection* section of the methods.
1248

1249 **Supplemental Figure 14**

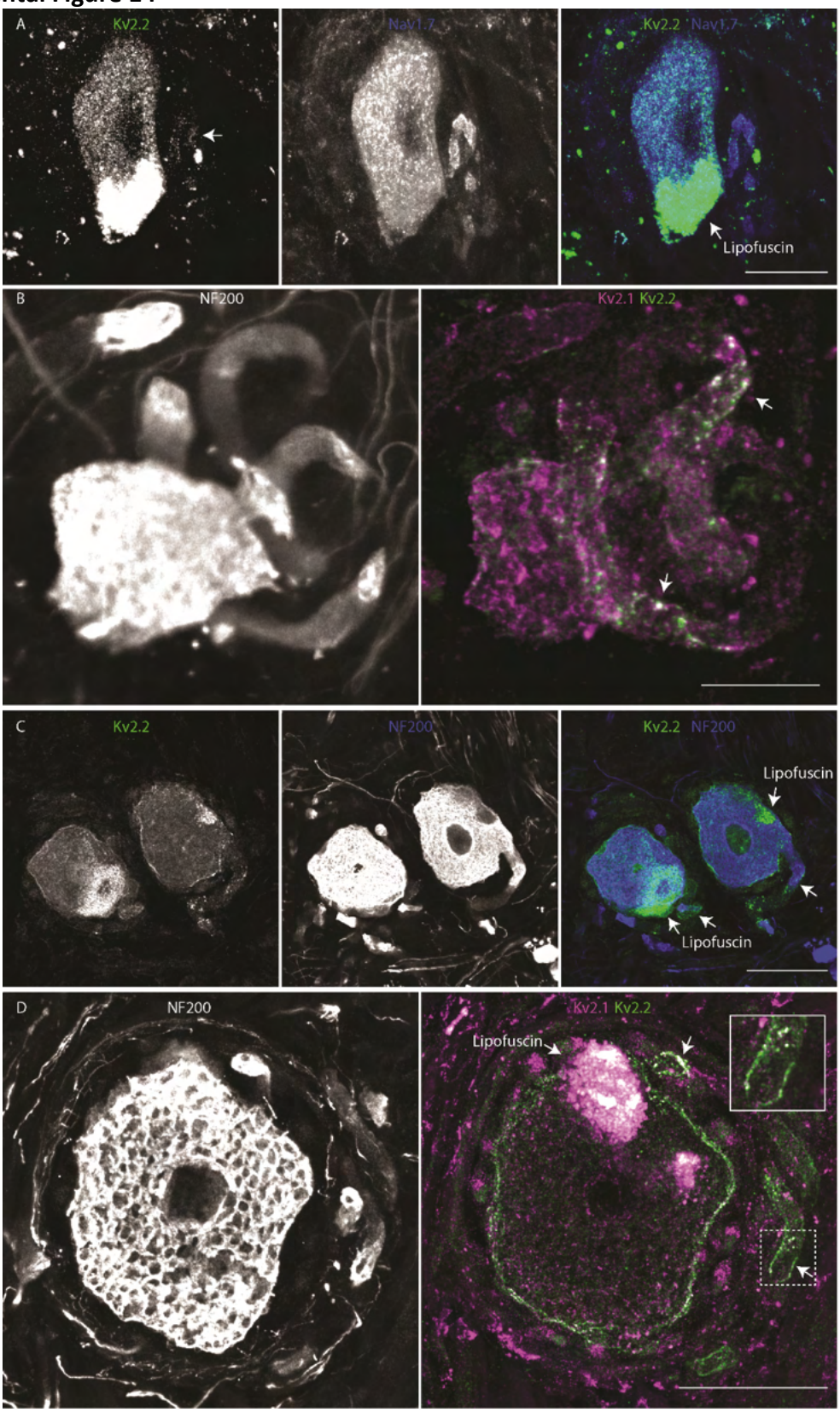

1250
1251

1252 **Supplemental Figure 14 legend**
1253 ***A***, Z-projection of anti-Kv2.2 and anti-Nav1.7 immunofluorescence in a human DRG neuron
1254 soma and stem axon. Arrow in merge indicates the stem axon of the DRG neuron. Apparent
1255 lipofuscin autofluorescence is labeled in merge. Image is from donor #2. Scale bar is 20 µm. ***B,***
1256 Z-projection of anti-Kv2.1 (magenta), anti-Kv2.2 (green) (right) and anti-NF200 (left)
1257 immunofluorescence in a human DRG neuron soma and stem axon. Arrows in merge indicate
1258 the stem axon of the DRG neuron. Image is from donor #1. Scale bar is 20 µm. ***C,*** Z-projection of
1259 anti-Kv2.2 (left) and anti-NF200 (middle) immunofluorescence in a human DRG neuron soma
1260 and stem axon. Arrow in merge indicates the stem axon of the DRG neuron. Apparent lipofuscin
1261 autofluorescence is labeled in merge. Image is from donor #1. Scale bar is 50 µm. ***D,*** Z-
1262 projection of anti-Kv2.1 (magenta), anti-Kv2.2 (green) (right) and anti-NF200 (left)
1263 immunofluorescence in a human DRG neuron soma and stem axon. Arrows in merge indicate
1264 the stem axon of the DRG neuron. Apparent lipofuscin autofluorescence is labeled in merge.
1265 Image is from donor #3. Scale bar is 50 µm. Detailed information on each donor can be found in
1266 the *Human Tissue Collection* section of the methods.
1267
1268
1269

1270 **Supplemental Figure 15**

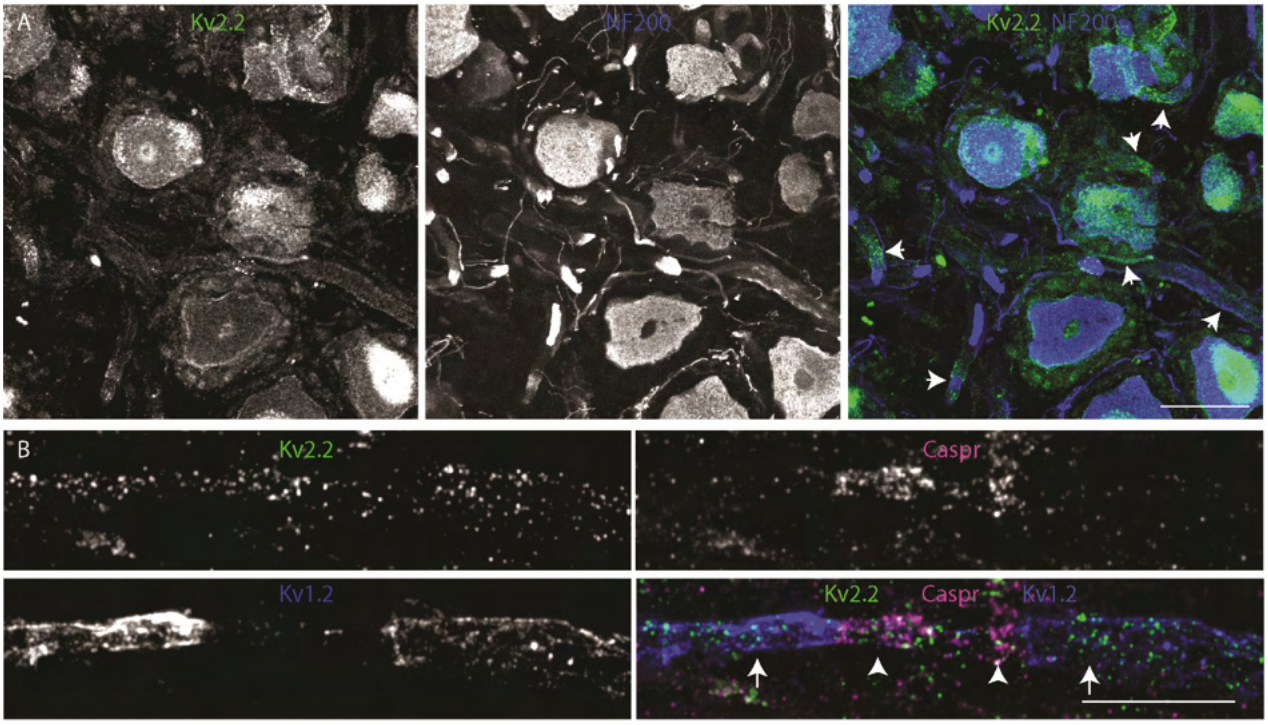

1271
1272 **Supplemental Figure 15 legend**
1273 ***A***, Z-projection of anti-Kv2.2 (left) and anti-NF200 (middle) immunofluorescence of human DRG.
1274 Arrows in merge represent exemplar axons which have clear anti-Kv2.2 immunofluorescence.
1275 Image is from donor #1. Scale bar is 50 µm. ***B***, Z-projection of anti-Kv2.2 (upper left), anti-CASPR
1276 (upper right) and anti-Kv1.2 (bottom left) immunofluorescence of human DRG axon. Image is
1277 from donor #2. Scale bar is 10 µm. Detailed information on each donor can be found in the
1278 *Human Tissue Collection* section of the methods.
1279
1280

1281 **TABLE 1**

Figure	Genotype	Number of Mice (N)	Sections/plates Analyzed	ROIs Analyzed (n)	Age (Weeks)	Sex	Level of spinal column	Total ROIs analyzed
1	WT	1	1	124	11	M	L	124
2	WT	5	3,4,10,8,4	52,172,476,437,134,	16,7,7,7,7	M,M,F,M,M	L,T12,T12,T12,T12	1271
	Kv2.1 KO	5	4,7,5,4,5	232,124,576,293,239,	16,7,7,7,7	M,M,F,M,M	L,T12,T12,T12,T12	1124
3	WT	8	4,11,4,6,4,4,4,6	238,126,1227,673,706,748,602,572,	50,50,50,7,7,24,7,28	M,M,M,M,M,M,M,F	L,T12,T12,T12,T12,T12,L1,T12	4892
	Kv2.2 KO	8	3,6,7,4,4,4,4,5	359,209,853,400,913,719,729,745,	50,50,50,7,7,24,7,28	M,M,M,M,M,M,M,F	L,T12,T12,T12,T12,T12,L1,T12	4927
4	WT	10	7,5,6,9,8	444,268,167,669,600,	50,50,50,50,50	F,F,F,M,M	T12,T12,T12,T12,T12	3419
	Kv2.1 KO	7	5,6	298,324,	50,50	M,M	T12,T12	622
	WT	8	same as data in figure 3					
	Kv2.2 KO	8	same as data in figure 3					
5	WT	3	4,16,17,	104,379,328,	18,19,19	F,F,F	L,L,L	811
	Kv2.1 Kv2.2 DKO	2	5,14,	108,274,	18,19	F,F	L,L	382
6	WT DRG	5	1,1,1,1,1	139,51,30,40,38	10,10,10,8,8	M,M,F,F,M	T12,T8,L1,L1,L1	298
	WT Ventral Horn	5	1,1,1,1,1	75,51,23,24,28	10,10,10,8,8	M,M,F,F,M	T12,T8,L1,L1,L1	201
7	WT	2	2	N/A	7,24	M,M	L1,T12	N/A
8	WT	1	1	N/A	7	M	L1	N/A
	Kv2.2 KO	1	1	N/A	7	M	L1	N/A
	MrgprD-GFP	1	1	N/A	13	F	T12	N/A
9	WT	1	1	N/A	28	F	T12	N/A
	Kv2.2 KO	1	1	N/A	28	F	T12	N/A
10	WT	1	1	N/A	10	M	L5	N/A
	MrgprD-GFP	4	6,5,9,14	852,632,842,1392,	13,20,8,8	F,M,F,F	T12,L1,L1,L1	3718
	WT	5	7,4,6,7,4	482,464,592,641,166,	7,10,24,19,19	F,M,M,F,F	L1,T12,T12,T12,T12	2345
	PV-tdTomato	2	15,9	1978,1158,	8,8	F,M	L1,L1	3136
1-1	WT	1	1	N/A	10	M	L5	N/A
1-2	WT	1	1	N/A	28	M	L	N/A

1-3	WT	1	3	125	13	M	L	125
2-1	WT	1	33	5399	8	M	T11 and T12	5399
2-2	MrgprDGFP	1	1	N/A	13	F	T12	N/A
2-3	MrgprDGFP	4	6,15,9,14	5,568,769,051,487	14,20,8,8	F,M,F,F	L1,L1,L1,L1	3824
	WT	2	7,5	771,478	24,8	M,F	L1,L1	1249
6-1	WT DRG	4	1,1,1,1	25,30,28,35	7,7,8	M,F,F,F	L1,L1,L1,L1	118
	WT Ventral Horn	4	1,1,1,1	17,19,26,19	7,7,8	M,F,F,F	L1,L1,L1,L1	81
7-1	MrgprDGFP	1	1	N/A	14	F	T12	N/A
	WT	2	1,1	N/A	11,17	M,M	L,L	N/A
8-1	WT	1	1	N/A	7	F	T12	N/A
	Kv2.1 KO	1	1	N/A	7	F	T12	N/A

Table 1 legend

Detailed information on mice used in each figure. In columns “Sections/Plates Analyzed”, “ROIs Analyzed”, “Age”, “Sex” and “Level of Spinal Column” information for each mouse is separated by commas. “ROIs Analyzed” corresponds to ROIs generated by automated analysis. In column “Level of Spinal Column” L1 refers to the first lumbar DRG and T12 refers to the twelfth thoracic DRG and if only L is shown the specific DRG is not known but the DRG is from the lumbar region.

1291 **TABLE 2**

Antigen	Antibody name	Species/isotype	Manufaturer information	Concentration used	RRID	Figures
Kv2.1	K89/34	Mouse IgG1 mAb	NeuroMab	6.7 ug/mL	AB_10672253	1, 2, 3, 4,6-1, 7, 8-1, 10, 11, 11-1, 11-2
Kv2.2	Kv2.2c	Rabbit pAb	In-house Trimmer laboratory	1:100 purified from strip assay	AB_2801484	3, 4, 6-1, 7, 8, 9, 10, 11, 11-1, 11-2,11-3
Nav1.8	N134/12	Mouse IgG2a mAb	NeuroMab	1:5 tissue culture supernatant	AB_10672261	1,11-1
Kv2.1	K89/34R	Mouse IgG2a mAb	In-house Trimmer laboratory	1:5 tissue culture supernatant	AB_2315768	11-1
beta III Tubulin	NA	Rabbit pAb	Abcam ab18207	0.33 ug/mL	AB_444319	2, 8-1
Kv2.2	N372B/60	Mouse IgG2b mAb	NeuroMab	1 ug/mL	AB_2315868	1, 1-3, 6, 10
NF200	NA	chicken pAb	Abcam ab4680	0.2 ug/mL	AB_304560	3, 8, 10
Caspr	K65/35	Mouse IgG1 mAb	NeuroMab	1:5 tissue culture supernatant	AB_2877274	9
Kv1.2	K14/16	Mouse IgG2b mAb	NeuroMab	1:5 tissue culture supernatant	AB_2877295	9,11
CGRP	NA	Rabbit pAb	Immunostar	1:1000	AB_572217	10
DsRed	NA	Rabbit pAb	Takara Cat#632543	0.17 ug/mL	AB_2307319	10
Nav1.7	N68/6	Mouse IgG1 mAb	NeuroMab	1:5 tissue culture supernatant	AB_2184355	11-1,11-3

1292

1293

1294 **Table 2 legend**

1295 Detailed information on antibodies used throughout the manuscript. In column “Concentration

1296 Used” if only dilution is given concentration was unknown however, tissue culture supernatant

1297 concentrations of antibodies typically range between 15-30 µg/mL.